ISBN 978-82-471-2519-9 (printed ver.)
ISBN 978-82-471-2521-2 (electronic ver.)
ISSN 1503-8181

Pamela Tempone

Doctoral Thesis

Doctoral theses at NTNU, 2011:6

Pamela Tempone

Effects of reservoir compaction on seismic and gravity monitoring

NTNU

Norwegian University of Science and Technology

Doctoral theses at NTNU, 2011:6

NTNU

NTNU
Norwegian University of Science and Technology
Thesis for the degree of philosophiae doctor
Faculty of Engineering Science and Technology
Department of Petroleum Engineering and Applied Geophysics

NTNU

Norwegian University of Science and Technology

Pamela Tempone

Effects of reservoir compaction on seismic and gravity monitoring

Thesis for the degree of philosophiae doctor

Trondheim, February 2011

Norwegian University of
Science and Technology
Faculty of Engineering Science and Technology
Department of Petroleum Engineering and Applied Geophysics

NTNU
Norwegian University of
Science and Technology

NTNU
Norwegian University of Science and Technology

Thesis for the degree of philosophiae doctor

Faculty of Engineering Science and Technology
Department of Petroleum Engineering and Applied Geophysics

ISBN 978-82-471-2519-9 (printed ver.)
ISBN 978-82-471-2521-2 (electronic ver.)
ISSN 1503-8181

Doctoral Theses at NTNU, 2011:6

Printed by Tapir Uttrykk

Licinius, trust a seaman's lore:
Steer not too boldly to the deep,
Nor, fearing storms, by treacherous shore
Too closely creep.

Who makes the golden mean his guide,
Shuns miser's cabin, foul and dark,
Shuns gilded roofs, where pomp and pride
Are envy's mark.

With fiercer blasts the pine's dim height
Is rock'd; proud towers with heavier fall
Crash to the ground; and thunders smite
The mountains tall.

In sadness hope, in gladness fear
'Gainst coming change will fortify
Your breast. The storms that Jupiter
Sweeps o'er the sky

He chases. Why should rain today
Bring rain tomorrow? Python's foe
Is pleased sometimes his lyre to play,
Nor bends his bow.

Be brave in trouble; meet distress
With dauntless front; but when the gale
Too prosperous blows, be wise no less,
And shorten sail.

Book II, Odes X, Horace
(Conington, 1882)

Abstract

The compacting reservoir embedded in a homogeneous, isotropic and elastic medium, known as Geertsma's model, is a model commonly used in feasibility studies for forecasting time-lapse changes due to hydrocarbon production. The scope of the thesis is to include a rigid basement to Geertsma's formulation, and to study how breaking the model symmetry affects the estimated changes in reservoir monitoring. The objective of introducing the rigid basement is to capture a general increase in rock stiffness with depth. In this way, the model narrows the gap between the analytical modelling and the effective deformation of the rocks surrounding the reservoir . The ultimate goal is to get a better estimation of the time-lapse changes expected from reservoir compaction.

An analytical solution for the displacement field caused by the compacting reservoir above a rigid basement is derived. The analytical model is introduced in a forward model for forecasting time-lapse changes in seismic monitoring and gravity monitoring. The results obtained in this way are compared with those obtained using Geertsma's model for the same forward model.

The most visible effects of the presence of the rigid basement are the increase of subsidence and the lowering of the top reservoir. Relevance should be also given to the increase of vertical stretching in the overburden and a corresponding stretching decrease in the underburden. In the time-lapse seismic modelling, these effects result in higher time-shifts in the overburden and lower in the underburden. In the time-lapse gravity modelling, the redistribution of the rocks around the compacting reservoir above the rigid basement causes a visible change in gravity, otherwise negligible in the homogeneous half-space.

By extending Geertsma's solution with a rigid basement below the compacting reservoir, the thesis provides a model that can reproduce the geomechanical behaviour of a subsurface where rock stiffness increases with depth. The model needs few parameters, and it can be implemented in a code that uses Geertsma's solution. A feasibility study that includes the rigid basement

model could bring interesting information to be taken into consideration in production management.

Acknowledgements

I am deeply grateful to my supervisors, Professor Martin Landrø and Professor Erling Fjær, for all help and recommendation through my Ph.D. path. Walking the Ph.D. path side by side with them, I discovered how scientific research is the result not only of a scrupulous application of the scientific method, but also a formulation of new ideas through an "artistically creative imagination" (Planck, 1949).

Acknowledgements go to Total E&P Norge for financial support of my Ph.D. work. Ottar Minsaas, Pascal Morin, Ying Guo, Jon Kleppe are acknowledged for interesting meetings between Total and NTNU, Norwegian University of Science and Technology.

Financial support has been also provided by the Norwegian Research Council through the Strategic University Program "ROSE", and the Project "History Matching using 4D Seismics and Production Data".

I acknowledge NTNU too for financial support through the Project "History Matching using 4D Seismics and Production Data".

I would like to thank Professor Sergio Fontura and his colleagues at the Group of Petroleum Technology and Engineering (GTEP) of the *Pontificia Universidade Católica* in Rio de Janeiro, for giving me the opportunity to join them and research temporarily in their department. A special thanks is for Nelson Inoue, who gave me valuable guidance in finite-element modelling.

I am grateful to Torkjell Stenvold for critical review of the paper included in Chapter 5. His comments gave me input for valuable improvement of the research method and the results presentation.

I thank Statoil for giving me access to some data on Kristin field. Understanding some of the problems related to real data manipulation will be very useful in my future career.

I thank Sintef Petroleum Research for giving me the opportunity to join temporary their seismic department and to get access to the software TIGER. I especially thank Michael Jordan for his supervision in finite difference modelling.

All my friends and colleagues at the Department of Petroleum Engineering and Applied Geophysics are acknowledged for sincere support and interesting discussions on practical issues on coding, on being Ph.D. candidate, and much more. I will particularly mention my office mates, Lyubov Skopintseva and Andreas Evensen, and the participant of the MBA (Alexey Stovas, Amir Ghaderi, Hossein Mehdizadeh, Milana Ayzenberg, Tor Erik Rabben).

A sincere thank you is to my friends, Mércia and Benjamin, who shared with me all the stages of my research, and always encouraged me.

A warm thank you is for my mum Anna Maria, my dad Francesco, and my brother Andrea for caring for me, and for supporting my choices.

Weider, thank you for your love.

List of Contents

List of Figures

Nomenclature

Roman Symbols

A	Crack area
a	Point source radius
A_g	Constant
c	Depth of reservoir
c_f	Fluid compressibility
C_m	Uniaxial compaction coefficient
E	Young's modulus
E_{fr}	Young's modulus, rock frame
f_1	Axial load on node 1
f_2	Axial load on node 2
G	Shear modulus
g_{Bpl}	Bouguer plate approximation
g_{FA}	Free-air correction
g_z	Vertical component of gravity
H	Reservoir thickness
h	Thickness of Bouguer plate
K	Bulk modulus
k	Depth of rigid basement

k_e	Stiffness of finite element
$K_{f,i}$	Bulk modulus, fluid component $i = 1 \cdots 3$
K_{fr}	Frame modulus
K_f	Bulk modulus, fluid
K_s	Bulk modulus, solid part
N	Number of nuclei
n	Number of crack per unit volume
N_c	Average number of contact per sphere
P	Coordinates of arbitrary point
p	Pore pressure
P_0	Observation point
Q_G	Inclusion impact parameter, shear modulus
Q_K	Inclusion impact parameter, bulk modulus
R	Distance between observation point and element volume
r	Radial axis
r_0	Radial coordinate of P_0
r_c	Distance between centre of mass and P_0
r_l	Dimension of the model in r-direction
R_s	Sphere radius
R_1	Distance between nucleus of stain and P
R_2	Distance between image nucleus of strain and P
S_i	Saturation, fluid component $i = 1 \cdots 3$
t	Seismic travel-time
u	Vertical displacement
u_0	Vertical displacement at $z = 0$
$u_{0,G}$	Free surface vertical displacement, Geertsma's model

$u_{0,MT}$ Free surface vertical displacement, McTigue's model

$u_{0,M}$ Free surface vertical displacement, Mogi's model

$u_{0,RB}$ Free surface vertical displacement, Rigid basement model

u_1 Displacement of node 1

u_2 Displacement of node 2

u_e Deformation of finite element

U_{res} Vertical displacements, whole reservoir

V Element volume

v Horizontal displacement, y-direction

v_0 Horizontal displacement at $z = 0$, y-direction

V_p P-wave velocity

V_{res} Horizontal displacements in y-direction, whole reservoir

V_s S-wave velocity

w Horizontal displacement, x-direction

w_0 Horizontal displacement at $z = 0$, x-direction

W_{res} Horizontal displacements in x-direction, whole reservoir

x Horizontal axis, x-direction

x_0 Horizontal coordinate of P_0, x-direction

$x_1, y_1, z_1, x_2, y_2, z_2$ Corner coordinates of Nagy's prism

y Horizontal axis, y-direction

y_0 Horizontal coordinate of P_0, y-direction

z Vertical axis

z_0 Vertical coordinates of P_0

Greek Symbols

β Ratio between frame compressibility and bulk rock compressibility

$\Delta\rho$ Change in fluid density

Δg Change in gravity

Δg_{FA} Change in free air correction

Δg_{res} Change in gravity due to saturation change

Δg_{wt} Change in gravity due to change in groundwater-table depth

$\Delta g_{z,ijt}$ Change in gravity of the element volume ijt, $i = 1, \cdots, mr$, $t = 1, \cdots, m\theta$ and $j = 1, \cdots, mz$

ΔH Change in reservoir thickness

Δp Change in reservoir pressure

ΔS_f Change in fluid saturation

Δt Time-lapse time-shift

ΔV Change in volume

Δz Change in depth

$\Delta \phi$ Change in porosity

$\Delta \rho$ Change in density

$\Delta \rho_f$ Change in fluid density

$\Delta \rho_{perm}$ Change in density of a permeable rock

δ_{ij} Kronecker delta

γ Crack aspect ratio

γ Shear strain

ν Poisson's ratio

ν_{fr} Poisson's ratio, rock frame

Φ Displacement potential

ϕ Porosity

Π Crack perimeter

ψ Harmonic functions

ρ Density

ρ_f Density, fluid

ρ_s Density, solid part

ρ_w Density of water

$\rho_{f,fin}$ Fluid density, final state

$\rho_{f,ini}$ Fluid density, initial state

$\rho_{f,i}$ Density, fluid component $i = 1 \cdots 3$

ρ_f Density, fluid

ρ_{mc} Density after production, mass conserved

ρ_s Density, solid material

σ_p External hydrostatic stress

σ_{ij} Stress component

θ First stress invariant

ε Normal strain

ε_{ij} strain component

ε_{vol} Volumetric strain

ζ Crack density

Subscripts

$_G$ Geertsma's model

$_r$ Radial direction

$_s$ Discretization index in r-direction

$_x$ x direction

$_y$ y direction

$_z$ Vertical direction

$_\theta$ Angular direction

$_b$ Base survey

$_{fin}$ State of the system after production

$_{ini}$ State of the system before production

$_{m}$ Monitor survey

$_{RB}$ Rigid Basement model

$_{s}$ System number, $s = 1 \cdots 3$

Other Symbols

$\mathbf{f}$ Vector function

$\mathbf{k}$ Unit vector in z-direction

$\mathbf{r}$ Vector distance between element volume and P_0

$\mathbf{R}_1$ Vector distance between nucleus of stain and P

$\mathbf{R}_2$ Vector distance between image nucleus of strain and P

$\mathbf{u}$ Displacement vector

$\mathbf{u}_G$ Displacement vector, Geertsma's model

$\mathbf{u}_{RB}$ Displacement vector, Rigid basement model

$\mathcal{G}$ Gravitational constant

$\mathcal{R}$ Dilation factor

J Bessel function

$\widehat{xz}$ Stress component, xz-plane

$\widehat{yz}$ Stress component, yz-plane

$\widehat{zz}$ Stress component, z-direction

Acronyms

FEM Finite element method

G Geertsma's model

RB Rigid basement model

Chapter 1

Introduction

The scope of my four years research is explained in the following sections. The summary of the main literature review related to my research leads to the motivation and the objectives of my work. The introduction continues with the research method used in the investigation and a summary of the results obtained. The chapter concludes with the outline of the dissertation and a summary of the contribution of each authors to the attached papers.

1.1 Scope of the thesis

Reservoir compaction is a rock mechanical phenomenon often observed during pressure depletion due to hydrocarbon production. The consequences of it affects different areas of hydrocarbon production and reservoir management. First, under given conditions, compaction can result in visible free surface subsidence, arising safety issues related to platform stability and environmental impact. Second, the rock adjustment to the change in reservoir volume, causes a stress and strain redistribution of the subsurface, often leading to collapse of well casing. Third, stress and strain redistribution increases the noise observed in geophysical monitoring. Forth, reservoir compaction can represent an important mechanism for hydrocarbon production.

One of the conditions for visible compaction is the significant reduction of pore pressure into a loose or weakly cemented rock, as observed in Groningen field (Mobach and Gussinklo, 1994). Another one is pressure depletion of high pressure high temperature reservoir (HPHT), as observed in Elgin-Franklin field (Hawkins et al., 2007). A further condition for compaction is the chemical interaction between reservoir formation and injected water, as observed in the

Ekofisk field (Teufel et al., 1991; Janssen et al., 2006; Guilbot and Smith, 2002) and in the Valhall field the North sea (Barkved et al., 2005).

Through the formulation and the solution of the theory of poro-elasticity, Geertsma (1966, 1973a,b) presents a simple method for the estimation of the reservoir compaction and the accompanying subsidence. The method, known as Geertsma's model, is based on the concept of *nucleus of strain*, a solution approach borrowed from thermo-elastic (Nowacki, 1986). The assumptions behind the model are that the reservoir is embedded in a homogeneous, isotropic, elastic medium and that the reservoir and the surroundings have the same elastic properties.

One of the main advantages of Geertsma's model is the low number of parameters required for the computation of displacements. Another one is the property of summation of the nucleus of strain that allows to cover all shapes of reservoirs (Geertsma and Van Opstal, 1973). However, an important limitation of the model is the assumption of homogeneity and linear elasticity, conditions not always found in sedimentary rocks.

A way to break the homogeneity of Geertsma's model is to introduce a rigid basement at arbitrary depth below the compacting reservoir. For this case, van Opstal (1974) provides the mathematical formulas for reservoir compaction and free surface subsidence. The extension of van Opstal (1974)'s formulas to the whole subsurface can be found in the work by Tempone et al. (2010a), included in the Chapter 3 of this thesis. The alternative to the analytical solution is the numerical modelling, for example using the finite-element method (FEM). The advantage of the numerical modelling is the flexibility of the model settings, however the main drawback is the increase in time for model building and computation.

Geophysical monitoring provides reservoir management with important information of changes happening inside a producing reservoir, in space and time. The risk related to geophysical monitoring is partly assessed through a feasibility study, that models the geophysical changes that are expected from production, and determines whether and how the changes can be observed. Once the time-lapse data are available, the same models can be updated and constrained to match the data, providing useful information to the reservoir engineers.

Although the initial application of Geertsma's model is the prediction of free surface subsidence, it has been very useful to improve the knowledge in the area of geophysical monitoring of a compacting reservoir. Important applications of the model for this purpose are in seismic and gravity monitoring.

In time-lapse seismic, Hatchell and Bourne (2005b) used the model to demonstrate the relation between the observed time-lapse changes in seismic traveltime to overburden stretching due to reservoir compaction. Another useful application is the integration of Geertsma's model into an inversion algorithm aimed to map pressure changes inside the producing reservoir using the observed time-lapse seismic time-shifts (Hodgson et al., 2007).

In time-lapse gravity, measured subsidence are compared with that one predicted by Geertsma's model with the purpose of detecting anomalous surface displacements and of inverting for reservoir compressibility (Stenvold et al., 2008; Stenvold, 2008; Eiken et al., 2008). This procedure leads ultimately to a better estimation of time-lapse gravity response, hence an improved knowledge of the reservoir changes at the reservoir level.

1.2 Motivation and objectives

One of the main limitations of Geertsma's model, as previously stated, is the assumption of homogeneity of the medium. This dissertation is motivated by a desire to include an heterogeneous component to Geertsma's model, and to study how this heterogeneity affects time-lapse geophysical modelling.

Existing time-lapse geophysical models prefer the use of analytical solutions because of the low number of parameters needed for the computation. Based on this observation, I decided to use an analytical solution to address the problem of the heterogeneity of the subsurface.

The heterogeneity studied in this dissertation is represented by a step increase of rock stiffness at an arbitrary depth, and deformation is not allowed below this rigid layer. In reality, it is difficult to find rigid surface in the Earth subsurface, however this model may fairly reproduce the displacement of a subsurface where stiffness increases with depth.

A further motivation that oriented the research is the interesting set that Geertsma's model and the Rigid basement model form together. Although both models are idealized geologies, they may be considered two extremes of the reality behaviour. The Rigid Basement model, for example, may be considered the upper bound for the subsidence, and Geertsma's model the lower bound. This statement is, however, limited by the know assumptions of elasticity and isotropy used in both models.

Based on the discussion above, the research aims to achieve the following main objectives:

- To provide formulas for displacement and stress of the subsurface rocks due to a compacting reservoir above a rigid basement.
- To introduce the Rigid Basement model into a forward model for prediction of time-lapse time-shifts and time-lapse gravity changes.
- To compare the results predicted with Geertsma's model and the Rigid Basement model.

1.3 Research method

The formulas for the Rigid Basement model are derived following the method presented by Sharma and Pilani (1956). Due to a hidden error in the mentioned paper, the formulas needed to be checked and re-derived, see also van Opstal (1974). The mathematical software Maple 11, distributed by Maplesoft, was one of the tools employed for helping in this purpose.

The numerical computation of the results is achieved implementing the equations of Geertsma's model and the Rigid Basement model in a MATLAB code. The results are validated using the solution for subsidence by van Opstal (1974) and a finite element model. The same code include the forward modelling of time-lapse time-shifts and time-lapse gravity changes. Time-lapse time-shifts are predicted through the strain model proposed by Hatchell and Bourne (2005a) and Røste et al. (2007, 2006), summarized in the next chapter. Changes in gravity are computed using the point mass approximation, explained more in detail in the next chapter.

1.4 Principal results and validation

The most visible effects of the presence of the rigid basement are the increase of subsidence and the lowering of the top reservoir, see the sketch in Fig. 1.1. The increased subsidence is confirmed by the results obtained with the formulas proposed by van Opstal (1974) and with a finite element modelling of the reservoir above a rigid basement, see Chapter 3 and Chapter 4 for more details.

Relevance should also be given to the increase of vertical stretching in the overburden and decrease in the underburden. In the time-lapse seismic modelling, these effects results in higher time-shifts in the overburden and lower in the underburden. A decrease in time-shifts in the underburden is observed

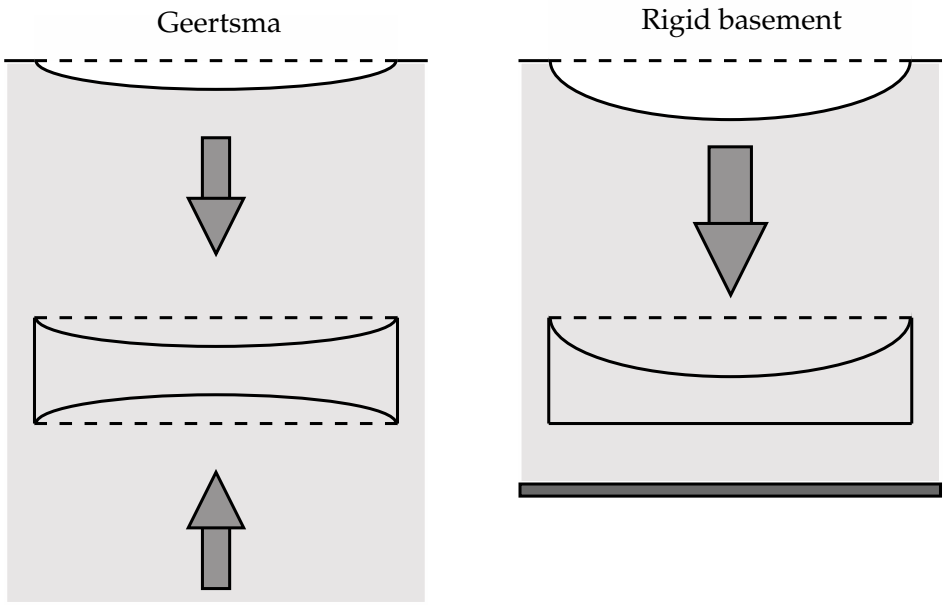

Figure 1.1: Sketch of rock displacements due to reservoir compaction in Geertsma's model and in the Rigid Basement model.

in Shearwater field by Staples et al. (2007), and a decrease in velocity in the underburden has been observed in the Valhall field by Hossein Mehdizadeh (personal communication, 2010).

In the time-lapse gravity modelling, the redistribution of the rocks around the compacting reservoir above the rigid basement causes a visible change in gravity, otherwise negligible in the homogeneous half-space (Bonaccorso et al., 2005; Battaglia et al., 2008). The finding of this dissertation are in agreement with those presented by Currenti et al. (2007).

1.5 Thesis outline

This chapter provides a brief overview of the background material, leading to the motivation and objectives of this research. The introduction continues with the research method and a summary of the results.

Chapter 2 summarizes the theory applied in the chapters that are coming. An overview of the geomechanical models relevant for the thesis is presented. This include Geertsma's model and finite element method. A summary of the

most common theories of rock physics is included, with the purpose of showing the link between reservoir production and geophysical changes. A description of the two geophysical monitoring methods used in the thesis, seismic and gravity, is given.

Chapter 3 presents the formulas for displacement and stress of the model extension of Geertsma's solution by adding a rigid layer beneath the compacting reservoir. The derivation includes the correction of an error found in the paper written by Sharma and Pilani (1956). The research included in Chapter 3 is published in *Applied Mathematical Modelling*, with the article title "Improved Solution of Displacements due to a Compacting Reservoir over a Rigid Basement". The paper was submitted in March 2009, and the revised version was submitted in February 2010. The first author derived and implemented the formulas for the Rigid Basement model, and wrote the article; the second and the third author supervised critically the research work; the question posed by the third author "What if we have a rigid basement?" gave the idea for the work.

Chapter 4 contains the paper "Effects on Time-lapse Seismic of a Hard Rock Layer beneath a Compacting Reservoir" by Tempone et al. (2009). This work was prepared for presentation at the 2009 SPE EUROPEC/EAGE Annual Conference and Exhibition held in Amsterdam, The Netherlands, 8–11 June 2009. The work describe how the analytical solution presented in Chapter 3 can be applied to model seismic time-shifts. The first author implemented the forward model for seismic monitoring, and wrote the article; the second and the third author supervised critically the research work; the forth author gave useful guidance in finite element modelling.

Chapter 5 contains the paper "4D Gravity Response of Compacting Reservoirs" by Tempone et al. (2010b), submitted to *Geophysics* in September 2010. The work includes the geomechanical modelling formulated in Chapter 3 in forward modelling for the estimation of change in gravity due to reservoir compaction. A parametric study on geometrical and geomechanical parameters is included. The first author defined the research method, implemented the forward model for gravity monitoring, and wrote the article; the second author gave the idea for the work; the third author provided fundamental guidance in defining the rock physical method; the second and the third author supervised critically the research work.

Chapter 7 closes the thesis with the conclusions and some closing remarks on the work presented in the previous chapters.

Chapter 2

Literature review

The prediction of the 4D signal of repeated seismic or gravity surveys due to reservoir compaction, requires the application of a set of theoretical or empirical models that represent the behavior of the subsurface. Three disciplines are the source of the models used in this research: geomechanics, rock physics and geophysics.

Geomechanics is the science that studies the mechanical behavior of soils and rock masses under forces and stress fields. In this research, geomechanics provides the theory and the tools for the estimation of the stress and the strain fields of the rocks of the subsurface due to reservoir compaction. Rock physics links the physical properties of the rocks and the geophysical observables. It provides the principles and the models to relate strain field and 4D seismic and 4D gravity. Geophysics, then, studies the physics of the Earth and its surroundings. Seismic and gravity theories have been used in the research in order to predict the 4D signal.

The following sections summarize the main concepts and the models of these disciplines that form the fundation of the PhD research.

2.1 Modelling of reservoir compaction

Hydrocarbon withdrawal causes depletion of fluid pressure inside the reservoir. If the rocks are loose and weak, the increase of effective stress may lead to compaction of the reservoir formation. Furthermore, propagation of the compaction through the surrounding rocks may result in visible free surface subsidence.

Prediction of reservoir compaction and surrounding deformations is a problem of rock mechanics, which has been solved with different methods within the petroleum industry. The following sections are aimed to summarize some of the known approaches for modelling reservoir compaction.

Ground deformation is an observed phenomena in volcano monitoring too. Solution for ground deformation provided in this discipline, can be very similar to those used in reservoir rock mechanics. Section 2.1.3 aims to point out some modelling similarities.

2.1.1 Uniaxial compaction

The simplest model for the estimation of reservoir change in volume is the uniaxial compaction model. It takes into consideration a reservoir that compact only vertically, as sketched in Fig. 2.1. Under the assumption of linear poro-elasticity, homogeneity and isotropy of the reservoir rocks, a simple expression for the change in vertical thickness, ΔH, can be formulated as:

$$\Delta H = \Delta p \cdot C_m \cdot H \tag{2.1}$$

where Δp is the pressure drop, and H is the initial thickness of the reservoir. C_m is the uniaxial compaction coefficient defined as:

$$C_m = \frac{1}{E_{fr}} \cdot \frac{(1+\nu_{fr}) \cdot (1-2\nu_{fr})}{1-\nu_{fr}} \tag{2.2}$$

where E_{fr} and ν_{fr} are the Young's modulus and the Poisson's ratio of the rock frame, respectively.

The formula Eq. 2.1 can be used for the estimation of the free surface subsidence, if we assume constant vertical stress acting on the reservoir. However, observation shows that subsidence is lower than the reservoir change in thickness, leading to the conclusion that the uniaxial reservoir compaction oversimplifies the geomechanical problem. An attempt to address the problem in an analytical way is represented by the poro-elastic theory outlined and solved by Geertsma (1966), and summarized in the following section.

2.1.2 Nucleus of strain method

The poro-elastic theory, formulated by Geertsma (1957, 1966), addresses the rock mechanical problem of reservoir compaction due to production pressure depletion through the stress–strain relation:

$$\sigma_{ij} = 2G \cdot \left(\varepsilon_{ij} + \frac{\nu}{1-2\nu} \cdot \varepsilon_{vol} \cdot \delta_{ij} \right) - (1-\beta) \cdot p \cdot \delta_{ij} \tag{2.3}$$

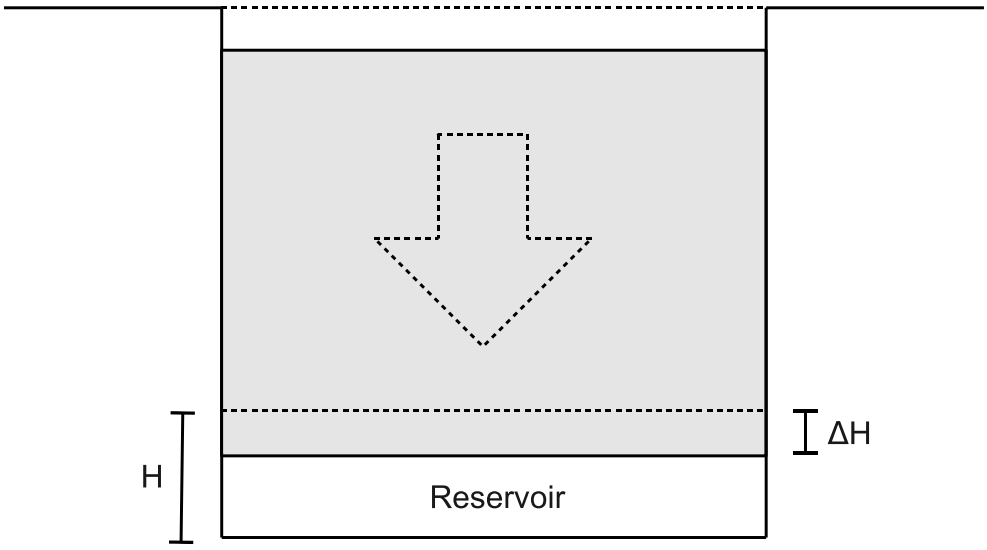

Figure 2.1: Uniaxial compaction model.

where σ_{ij} is the stress component, ε_{ij} is the strain component, ε_{vol} is the volumetric strain, G is the shear modulus, ν is the Poisson's ratio, β is the ratio between frame compressibility and bulk rock compressibility, and δ_{ij} is the Kronecker delta. p is the pore-fluid pressure.

The mathematical description of Eq. 2.3 for the theory of poro-elasticity is similar to that one used for the theory of thermo-elasticity, see Nowacki (1986). Geertsma takes advantage of this similarity using mathematical techniques already applied to solve thermo-elastic problems. The preferred method is that one that uses the concept of the *nucleus of strain* (Geertsma, 1973b, 1966, 1957).

The problem to be solved with the concept of the *nucleus of strain* is constituted by a compacting reservoir embedded in an homogeneous, isotropic and linear-elastic half space. Because the local change in strain and stress due to compaction, that is our main interest, leaves the gravity stress field unaffected, gravity load is neglected in the formulation and solution of the problem.

The method requires the discretization of the reservoir in element volumes, that contain a shrinking nucleus of strain. The displacement vector, $\mathbf{u}_G$, around a nucleus of poro-elastic strain of volume V at depth of burial c expe-

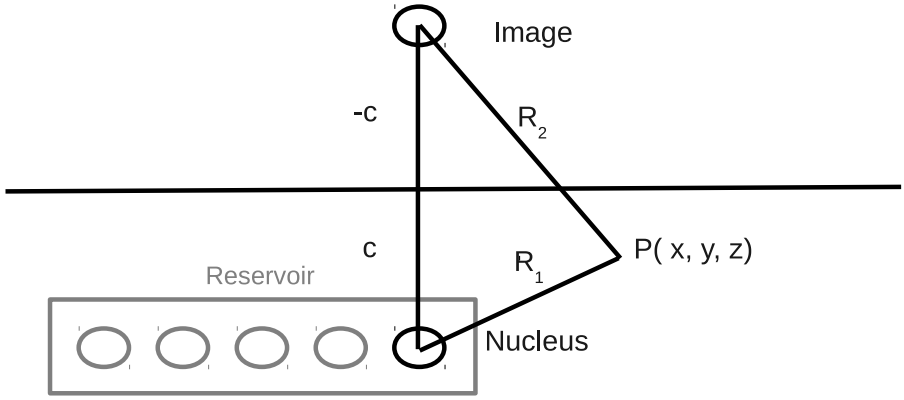

Figure 2.2: Sketch of the nucleus of strain concept.

riencing a pore pressure reduction Δp amounts to:

$$\mathbf{u}_G = \frac{C_m \cdot \Delta p \cdot V}{4\pi} \cdot \left\{ \frac{\mathbf{R}_1}{R_1^3} + \frac{(3-4\nu)\cdot \mathbf{R}_2}{R_2^3} - \frac{6z\cdot(z+c)}{R_2^5} - \right. \\ \left. - \frac{2\mathbf{k}}{R_2} \cdot [(3-4\nu)\cdot(z+c) - z] \right\} \tag{2.4}$$

where C_m is the uniaxial compaction coefficient, ν is the Poisson's ratio of the material, R_1 is the distance $\sqrt{r^2+(z-c)^2}$, and R_2 is the distance $\sqrt{r^2+(z+c)^2}$. The free surface subsidence, $u_{0,G}$, becomes:

$$u_{0,G} = \frac{C_m \cdot \Delta p \cdot V}{\pi} \cdot (1-\nu) \cdot \frac{c}{(r^2+c^2)^{3/2}} \tag{2.5}$$

Eq. (2.4) is defined in a cylindrical coordinate system, where r is distance on the radial axis and z is the depth. $\mathbf{k}$ is the unit vector in z-direction, and it is positive downward. The displacement field of a compacting reservoir is equal to the integration of Eq. (2.4) over the reservoir volume.

Geertsma's model predicts a lowering of overburden and an uplift of the underburden, as shown in Fig. 2.3(a). The top and the bottom of the reservoir displace almost equally downward and upward, respectively. The rock above the tips of the reservoir displace toward the centre of symmetry, as shown in Fig. 2.3(b). The overburden and the underburden are stretched vertically, whereas the sideburdens are compressed vertically.

The integration over the reservoir volume can be analytical or numerical. The analytical solution is available only for few geometrical configurations, e.g. cylindrical reservoirs. The alternative method is resorting to the numerical

integration of the contribution of small parts in which the reservoir volume can be discretized (Geertsma and Van Opstal, 1973). The accuracy of the numerical integration is dependent on the discretization size of the reservoir (Lewis et al., 1983).

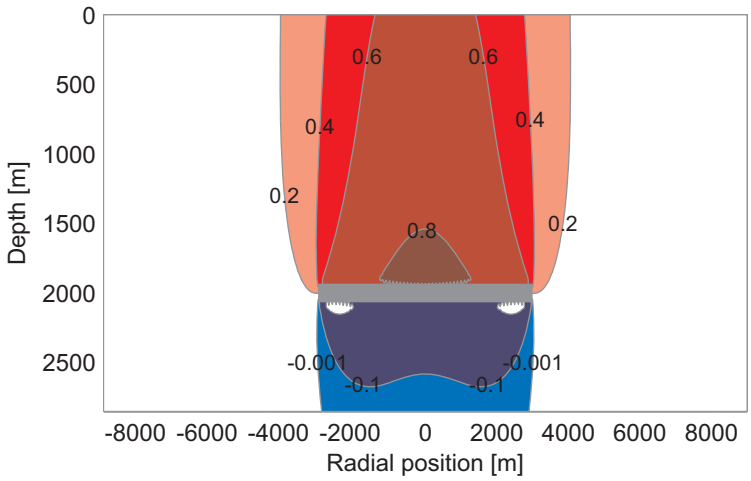

(a) Vertical displacement

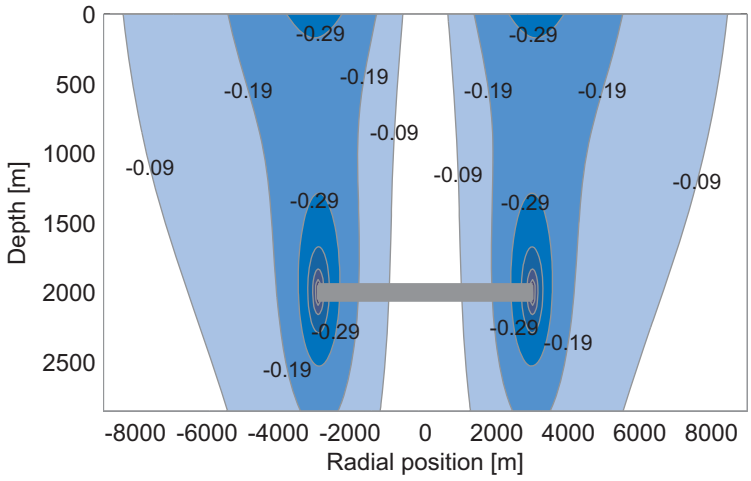

(b) Horizontal displacement

Figure 2.3: Vertical and horizontal displacement field due to a compacting reservoir. Geertsma's solution. Warm colours represent positive displacement, and cold colours negative displacements.

The strength of Geertsma's model is the low number of parameters needed

to get the estimation of compaction, subsidence and stress changes of the subsurface. However, the assumptions of homogeneity, isotropy and linear elasticity limits the range of application of the model. A way to address this problem is to introduce some condition of heterogeneity, like a stiffness contrast between reservoir and surroundings or a rigid basement below the reservoir.

An extension of Geertsma's model is provided by van Opstal (1974). The author incorporates a rigid basement at an arbitrary depth below the compacting reservoir. The formula representing the free surface subsidence in this condition is:

$$u_{0,RB} = \frac{1-\nu}{2\pi} \cdot C_m \cdot \frac{2 \cdot c}{\left(r^2 + c^2\right)^{3/2}} \\ \frac{1-\nu}{2\pi \cdot \sqrt{r}} \cdot C_m \cdot \int_0^\infty \lambda^{-1/2} \cdot C \cdot (\lambda \cdot r)^{1/2} \, \mathrm{J}_0 \left(\lambda \cdot r\right) \mathrm{d}\lambda \tag{2.6}$$

where:

$$C = \frac{\lambda}{2 \cdot \Delta} \left\{ e^{\lambda \cdot c} \cdot (2\lambda \cdot k + 1) - e^{-\lambda \cdot c} \cdot \left[4\lambda^2 \cdot k^2 + 2\lambda \cdot k + (3 - 4\nu)^2 \right] + \right. \\ \left. - (3 - 4\nu) \cdot \left(e^{-\lambda(2k+c)} - e^{-\lambda(2k-c)} \right) \right\} \tag{2.7}$$

$$\Delta = (1 - 2\nu)^2 + \lambda^2 \cdot k^2 + (1 - 4\nu) \cdot \cosh^2 (\lambda \cdot k) \tag{2.8}$$

and where k is the depth of the rigid basement, c is the depth of the reservoir, ν is Poisson's ratio, C_m is the uniaxial compaction coefficient, and r is the radial coordinate of an arbitrary point lying on the free surface. The formulas for the deformation of van Opstal (1974) are extended to the whole subsurface in Chapter 3.

The problem solved with poro-elasticity in reservoir rock mechanics is very similar to the problem of ground deformation observed in volcano monitoring. The following section is aimed to point out the similarities in the solution of the two field of application. The most important analytical solutions are listed and shortly compared to Geertsma's solution.

2.1.3 Analogies with volcano uplift modelling

The deformation of the free surface is a phenomenon observed in volcano monitoring too. Estimating surface deformation is an important tool necessary to discriminate magma transport at depth. Analytical models are traditionally

used for this purposes, and the most common is Mogi's point source (Mogi, 1958).

Mogi's point source solves the problem represented by an expanding or contracting magma chamber embedded in a homogeneous, isotropic and elastic half-space. The source of deformation is represented by a sphere with a radius significantly smaller than its depth. For this problem, the deformation of the free surface, $u_{0,M}$, is represented by the following formula:

$$u_{0,M} = \frac{3\Delta p}{4G} \cdot a^3 \cdot \frac{c}{\left(r^2 + c^2\right)^{3/2}} \tag{2.9}$$

where c is the depth of the point source, a is the radius of the source, Δp is the pressure change, G is the shear modulus of the model medium, and r is the radial coordinate of an arbitrary point on the free surface. Eq. 2.9 assumes a Poisson's ratio equal to 0.25.

The assumption that the source radius is small compared to the depth is addressed by McTigue (1987). The author provides an approximated analytical solution for displacement and stress. The mathematical method used for this purpose is the *method of reflection*, a known method in mechanical engineering. In this case, the formula for the displacement at the free surface, $u_{0,MT}$, is (Battaglia et al., 2008):

$$\begin{aligned} u_{0,MT} = \ & (1-\nu) \cdot \frac{\Delta p \cdot a^3}{G} \cdot \frac{c}{\left(r^2 + c^2\right)^{3/2}} \cdot \\ & \cdot \left\{ 1 - \left(\frac{a}{c}\right)^3 \cdot \left[\frac{1+\nu}{2\,(7-5\nu)} - \frac{15\,(2-\nu)}{4\,(7-5\nu)} \cdot \frac{c^2}{\left(r^2 + c^2\right)} \right] \right\} \end{aligned} \tag{2.10}$$

where the notation is the same as explained in Eq. 2.9.

The difference between Geertsma's solution for the subsidence, Eq. 2.5, and Mogi's one in Eq.2.9 is quantified by a factor dependent on Poisson's ratio, and is equal to:

$$\alpha = \frac{1-2\nu}{2\,(1-\nu)} \tag{2.11}$$

However, the solutions for the displacement of an arbitrary point in the subsurface are derived with different mathematical approaches, see Mindlin and Cheng (1950) for Geertsma's model and McTigue (1987) for Mogi's source. This difference may lead to differences in the predicted displacement and stress field due to pressure change of the source. It would be interesting to compare the general formulas for displacement and stress, though time constrains the research objectives.

An example of subsidence estimated with both Geertsma's and Mogi's models is presented in Fig. 2.4. The example consider a shrinking point source under a negative change in pressure of -10 MPa. The source is buried at 500 m and has a radius of 50 m. The model medium has Poisson's ratio equal to 0.25 and shear modulus equal to 1 GPa. It can be observed that graphs differ only in magnitude, while keeping the same shape, as already mentioned in the previous paragraph.

The assumptions lying behind the analytical solutions by Geertsma and Mogi introduce errors in the representation of reality, and they limit the range of application to simple geologies. A way to study complex geologies is to numerically model it, using finite element method for example. Next section summarizes the basic concept of this numerical tool.

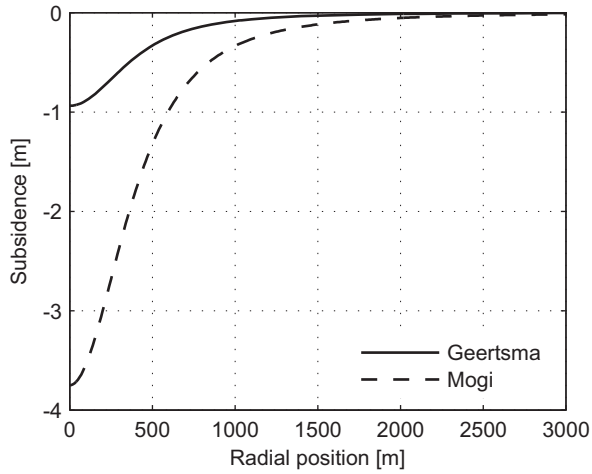

Figure 2.4: Subsidence obtained with Geertsma's model and Mogi's point source model.

2.1.4 Finite element method

The Finite Element Method (FEM) is a computational method for approximate solution of complex engineering problems. The basic concept of FEM is the decomposition of the domain of the problem into a finite number of elements interconnected by nodes. The unknowns related to each element are approximated through interpolation functions.

The linear spring system is a simple mechanical problem that can be used for the illustration of the FEM approach. In the one-dimensional domain, the

spring is composed by one element and two nodes, as schematized in Fig. 2.5. The nodes are displacing due to axial loads, f_1 and f_2. The deformation of the element, u_e, as function of the displacements of the nodes, u_1 and u_2, is expressed as:

$$u_e = u_1 - u_2 \tag{2.12}$$

The force acting on node 1 is related to the deformation of the element and its stiffness, k_e, by:

$$f_1 = k_e \cdot u_e = k_e \cdot (u_1 - u_2) \tag{2.13}$$

The system is in equilibrium if:

$$f_2 = -f_1 = k_e \cdot (u_2 - u_1) \tag{2.14}$$

The system of equations can be written in matrix form as:

$$\begin{bmatrix} k_e & -k_e \\ -k_e & k_e \end{bmatrix} \cdot \begin{Bmatrix} u_1 \\ u_2 \end{Bmatrix} = \begin{Bmatrix} f_1 \\ f_2 \end{Bmatrix} \tag{2.15}$$

Solving the system of equations 2.15 means estimating the displacement of the nodes 1 and 2, that is the objective of the modelling.

In the reservoir compaction problem, FEM is often coupled with a reservoir modelling of fluid flow. In this way, the reservoir rock deformation is directly linked to the pore volume change through a pore volume compressibility coefficient. In addition, the coupling is able to recreate the time dependent component of rock deformation related to fluid flow.

The advantage of the FEM model is the ability to take into consideration the spatial variation of the geomechanical properties of the rocks, inside and outside the reservoir. In order to exploit the modelling at its maximum, the geology and the spatial distribution of the rock properties in the subsurface has to be recreated as closely as possible to reality. On the other side, the time invested in model building and computation, increases side by side with the increase of details in the geomechanical model.

Geertsma's model, Mogi's model and FEM modelling are all geomechanical tools that can be used to estimate of the displacement and stress caused by reservoir compaction. However, ground deformation is only one of the time-lapse observations that we can collect to monitor the subsurface changes. Further observations come from seismic and gravity monitoring. In order to forecast such time-lapse changes due to compaction, we need models that link subsurface deformation to geophysical response. Rock physics is the discipline that provides those models. A summary of some of the rock physical models available is presented in the next section.

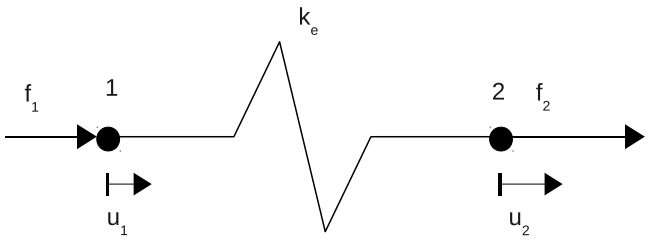

Figure 2.5: Sketch of a linear spring element.

2.2 Rock physics models

Rock physics is the science that aims to relate the geological properties of a rock at certain physical conditions, like pressure and temperature, with the corresponding elastic and seismic properties. For example, porosity, lithology and saturation are some of the geological properties, and elastic modulus, velocity and impedance are seismic properties.

The rock physics relations are used in seismic modelling, for example, to predict the elastic properties from geology, or in seismic inversion to predict geology from elastic observations. Rock physics is particularly useful when analysing time-lapse seismic as it allows the prediction of reservoir properties at various production states.

During production, the properties of the reservoir rocks vary in time due to a number of factors, like fluid substitution or pore pressure change. In the following sections, the most important relations that link density and elastic properties to change in pore pressure and fluid saturation are presented (Mavko et al., 1998; Calvert, 2005; Fjær et al., 2008).

2.2.1 Fluid substitution effects

Hydrocarbon production causes the flow of the reservoir fluids through the porous formation. The fluid displacement causes a change in saturation of the fluids within the pore volume. If we know the initial condition of the reservoir rocks and the final properties of the fluid, we are able to predict the final density and elastic properties of the rocks.

Density change The replacement of hydrocarbons with another fluid causes the change of the density of the reservoir rock. The initial density of a rock is expressed as:

$$\rho = \rho_f \cdot \phi + (1 - \phi) \cdot \rho_s \tag{2.16}$$

where ρ_f is the density of the fluid, ρ_s is the density of the solid part of the rock, that is assumed to be constant in time, and ϕ is the porosity of the rock. The pore fluid density is the weighted sum of the fluid components, expressed as:

$$\rho_f = \sum_i S_i \cdot \rho_{f,i} \tag{2.17}$$

where $\rho_{f,i}$ is the density of component i present with saturation S_i. Assuming that the porosity is constant, the simplest expression for the change in density, $\Delta\rho$, is :

$$\Delta\rho = \phi \cdot (\rho_{f,fin} - \rho_{f,ini}) \tag{2.18}$$

where $\rho_{f,ini}$ and $\rho_{f,fin}$ are initial and final density of the pore fluid, respectively.

Gassmann's substitution method Fluid substitution results in changes of bulk modulus of the rock, hence in changes of compressional wave velocity. The most widely used method for the estimation of the bulk modulus value due to fluid substitution is the Gassmann substitution method (Gassmann, 1951). The model estimates the bulk modulus, K, of a rock constituted by an assembly of grains through the equation:

$$K = K_{fr} + \frac{\left(1 - \frac{K_{fr}}{K_s}\right)^2}{\frac{\phi}{K_f} + \frac{1-\phi}{K_s} - \frac{K_{fr}}{K_s^2}} \tag{2.19}$$

where K_{fr} is the frame modulus, K_f is the fluid bulk modulus, and K_s is the bulk modulus of the solid part of the rock. The fluid bulk modulus of a fluid mix is dependent on the saturation, S_i, and on the bulk modulus, $K_{f,i}$, of the component i present in the rock:

$$\frac{1}{K_f} = \sum_i \frac{S_i}{K_{f,i}} \tag{2.20}$$

Eq. (2.19) can be used to estimate the bulk modulus before and after production in various production scenarios just substituting the initial and final bulk

modulus of the fluid mix. Once the bulk modulus is known, compressional, V_p, and shear, V_s, velocities can be computed from:

$$V_p = \sqrt{\frac{K + \frac{4}{3} \cdot G}{\rho}} \quad \text{and} \quad V_s = \sqrt{\frac{G}{\rho}} \tag{2.21}$$

where G is the shear modulus, that is independent from the fluid composition at low seismic frequencies. The velocities coming from Eq. (2.21) can be introduced in a synthetic seismic modelling for predicting time-shifts and amplitude changes due to production.

2.2.2 Pressure effects

Changes of fluid pressure causes redistribution of the effective stress inside the reservoir. Depending on the rock properties of the formation, compaction of the reservoir may occur causing a redistribution of the stress field of the surrounding rocks too. Different models are available for the prediction of the change in seismic properties caused by pressure changes.

Granular medium model The granular medium model is suitable for the determination of the bulk modulus of a rock composed by solid grains as function of external pressure. The theory has been first formulated by Hertz (1882), and then extended by Mindlin (1949) providing the basis for the Hertz-Mindlin contact model. The model provides with a formulation that relates the growth of the contact area a between two spheres, and the external load F, see Fig. 2.6 :

$$u = \sqrt[3]{\frac{9 \cdot \left(1 - \nu_s^2\right) \cdot F^2}{2 \cdot E_s^2 \cdot R_s}} \tag{2.22}$$

where u is the vertical displacement, E_s and ν_s are the elastic modulus and the Poisson's ratio of the spheres respectively, and R_s is the radius of the sphere. The model involve the calculation of the bulk modulus and shear modulus of two adjacent spheric grains as function of their radius and elastic moduli. Through averaging (Walton, 1987), then, the bulk modulus, K, of a pack of grains can be expressed by:

$$K = \sqrt[3]{\frac{N_c^2 \cdot (1 - \phi)^2 \cdot E_s^2 \cdot \sigma_p}{72 \cdot \pi^2 \cdot \left(1 - \nu_s^2\right)^2}} \tag{2.23}$$

and shear modulus, G, can be expressed by:

$$G = \frac{5 - 4 \cdot \nu_s}{10 \cdot (2 - \nu_s)} \cdot \sqrt[3]{\frac{3 \cdot N_c^2 \cdot (1 - \phi)^2 \cdot E_s^2 \cdot \sigma_p}{\pi^2 \cdot (1 - \nu_s^2)^2}} \tag{2.24}$$

where N_c is the average number of contact per sphere, ϕ is the porosity, and σ_p is the external hydrostatic pressure.

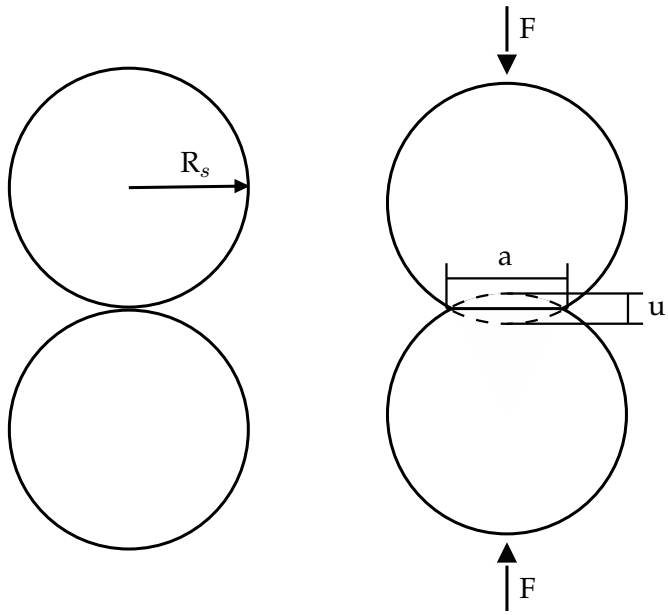

Figure 2.6: Sketch of the Hertz-Mindlin contact model.

Inclusion model The inclusion models is suitable for the representation of a continuous rock interrupted by holes or fractures with different shapes, as sketched in Fig. 2.7 (Fjær et al., 2008). In the isotropic case, the bulk modulus, K, and the shear modulus, G, can be expressed as functions of inclusion concentration by:

$$K = K_s \cdot (1 - Q_K \cdot \zeta) \tag{2.25}$$

$$G = G_s \cdot (1 - Q_G \cdot \zeta) \tag{2.26}$$

where K_s and G_s are , respectively, the bulk modulus and shear modulus of the solid material. If the inclusions are flat cracks, the term ζ is known as crack density and defined as the average:

$$\zeta = \frac{2 \cdot n}{\pi} \cdot \left\langle \frac{A^2}{\Pi} \right\rangle \tag{2.27}$$

where A and Π are the area and perimeter of a crack, respectively, and n is the number of cracks per unit volume. Q_K and Q_G are terms that take into consideration the impact of the inclusions on the solid rock. For cracks randomly oriented and filled with fluid, an expression for Q_K and Q_G is given by Budiansky and O'connell (1976):

$$Q_K = \frac{16}{9} \cdot \frac{1-\nu_s^2}{1-2\nu_s} \cdot D \tag{2.28}$$

$$Q_G = \frac{32}{45}(1-\nu_s) \cdot \left(D + \frac{3}{2-\nu_s} \right) \tag{2.29}$$

where ν_s is the Poisson's ratio of the solid material, and D is expressed as

$$\frac{1}{D} = 1 + \frac{4}{3\pi \cdot \gamma} \cdot \frac{1-\nu_s^2}{1-2\nu_s} \cdot \frac{K_f}{K_s} \tag{2.30}$$

where γ is the ratio between thickness and diameter of the cracks, and K_f is the bulk modulus of the pore fluid. The inclusion model can be extended to include stress dependency of the bulk modulus and shear modulus (Fjær, 2006).

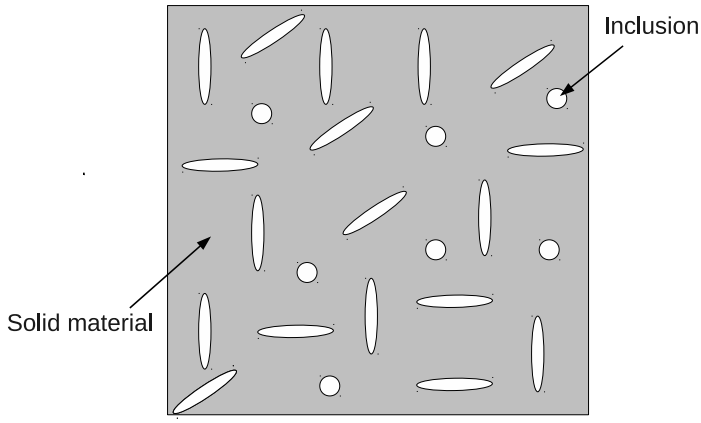

Figure 2.7: Inclusion model.

Empirical models Strain as result of changes of reservoir volume can directly impact velocity parameters inside and outside the reservoir. Hatchell and Bourne (2005b) and Røste et al. (2007, 2006) found that a factor, called dilation factor $\mathcal{R}$, is a convenient link between relative change in velocity, V_p, and vertical strain, ε_z in the overburden:

$$\frac{\Delta V_p}{V_p} = \mathcal{R} \cdot \varepsilon_z \tag{2.31}$$

Values for the dilation factor have been found empirically. According to Hatchell and Bourne (2005b), the dilation factor estimated from time-lapse seismic surveys is close to 5 if the rocks stretch, and between 1–3 if the rock compact. However, Holt et al. (2008) shows that the dilation factor estimated with lab measurements may be very different and strongly depend on the stress path applied to the core.

2.3 Geophysical monitoring

Geophysical reservoir monitoring permits us to estimate the changes in properties of hydrocarbon producing reservoirs, in space and in time. As the water takes the place of the hydrocarbons and as the pressure of the reservoir formation changes, the seismic velocity and the density of the rocks change. Repeated geophysical surveys of the reservoir before and during production, can capture when and where those changes are happening. Through an accurate analysis of the time-lapse surveys, we can estimate the changes inside the reservoir.

The knowledge of the place and the moment when changes take place inside the reservoir is the major objective of reservoir monitoring. Thanks to this knowledge, indeed, a better management plan of the reservoir can be defined and a recovery improvement is ultimately possible (Calvert, 2005). The optimal production of hydrocarbon reserves is becoming a crucial point of interest in a world where energy consumption is increasing exponentially and where new hydrocarbon resources are hard to be found (Lakatos and Lakatos-Szabo, 2009; Rogner, 1997).

Time-lapse technology includes different tools able to monitor the reservoir changes due to production. In the list of those tools are: time-lapse reflection seismic, microseismicity, time-lapse gravity, electromagnetic monitoring, and others. In my research work, I have been modelling the change of some of the reservoir parameters that may be detected in time-lapse seismics and time-lapse gravity. These two monitoring techniques are shortly described in the following subsections.

2.3.1 Time-lapse seismics

Repeated seismic surveys, before and during production, can provide important information on changes happening at the reservoir level. The measurement of the changes can be evaluated looking at the amplitude difference, δA,

or at the time-shift, δt, between base and monitor, see Fig. 2.8. However, the success of time-lapse seismics is dependent on accurate feasibility study and on data processing.

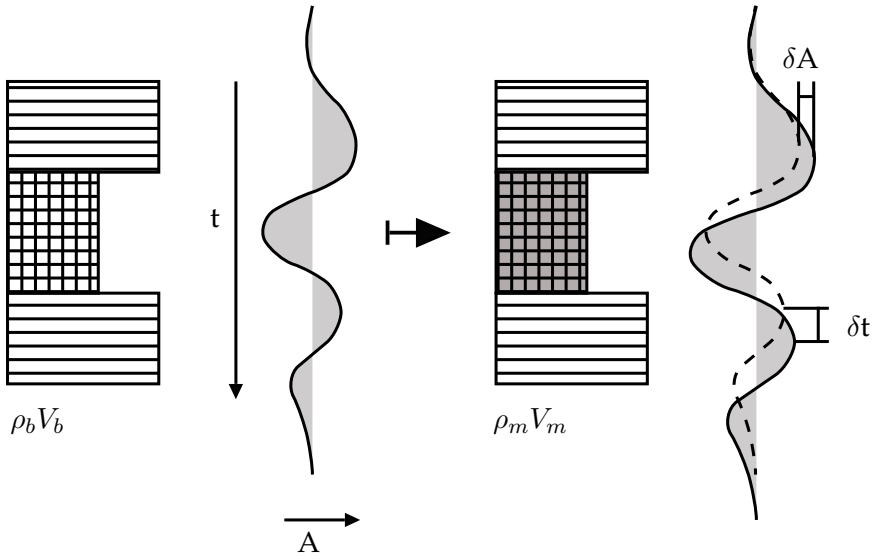

Figure 2.8: Changes in a seismic wave due to changes in rock properties.

Before the acquisition of the repeated surveys, a feasibility study should be carried out for the reservoir to be monitored, as summarized by Lumley et al. (1997). A number of parameters must be taken into consideration: reservoir parameters, such as depth and pore pressure, rock properties, such as porosity and rock bulk modulus, fluid properties, such as saturation change and density, seismic parameters, such as resolution and repeatability.

Feasibility modelling is a quantitative tool used to predict the magnitude of the time-lapse changes. We are interested in determining if the producing reservoir and its surrounding are prone to give visible changes.In order to succeed in our goal, we need relationships between rock properties changes and seismic properties, examples of such relations are listed in Section 2.2.

Amplitude difference By differentiating the monitor and the base surveys, we obtain the amplitude difference volume. The amplitude difference is a convenient method used in time-lapse interpretation, that permits to highlight changes at reservoir level by subtracting strong constant-in-time geological events. Changes are highlighted even in thin reservoirs. The display of the

map of the amplitude change at the reservoir level is a tool to detect where the fluids are moving (Eiken et al., 2000).

The measurement of the amplitude changes is also an important source of information for quantitative estimation of the change in fluid pressure and saturation inside the producing reservoir (Tura and Lumey, 1999; Landrø, 2001). Both pre-stack and post-stack data are useful for this purpose. Landrø (2001), for example, proposes approximate expressions for the estimation of saturation and pressure as function of Amplitude Versus Offset (AVO).

Time-shifts Because reservoir production causes change in rock velocity, the time needed by the waves to propagate within the Earth is different between base and monitor. Measuring the time-shifts and the correlation between the repeated surveys can be an important source of information for the discrimination of the changes localized at the reservoir level.

In the case of a compacting reservoir, for example, the seismic properties of the rock in the surrounding of the reservoir changes due to the arching effect. As a consequence of the rock deformation, the waves travel with a different speed already in the overburden, see Fig. 2.9. The time-shifts, Δt, due to the arching effect in the overburden, can be estimated through the formula proposed by Landrø and Stammeijer (2004):

$$\frac{\Delta t}{t} = \frac{\Delta z}{z} + \frac{\Delta V_p}{V_p} \tag{2.32}$$

where t is the wave travel time, z is the depth of the reflector, Δz is the change in depth of the reflector, V_p is the P-wave velocity of the rock above the reflector, and ΔV_p is the change in P-wave velocity due to rock redistribution in the reservoir surroundings. By correlating the base and the monitor surveys, it is possible to measure the time-shift differences above and below the reservoir. The changes localized inside the reservoir interval can be recognized, and a more accurate interpretation of the measurements can be carried out.

2.3.2 Time-lapse gravity

The total gravity change, Δg, at an observation point $P_0(x_0, y_0, z_0)$, can be expressed as the sum of four terms:

$$\Delta g\,(P_0) = \Delta g_{res} + \Delta g_{FA} + \Delta g_{def} + \Delta g_{wt} \tag{2.33}$$

where Δg_{res} is the change in gravity due to mass substitution and redistribution at the reservoir level, Δg_{FA} is the change in gravity dependent on

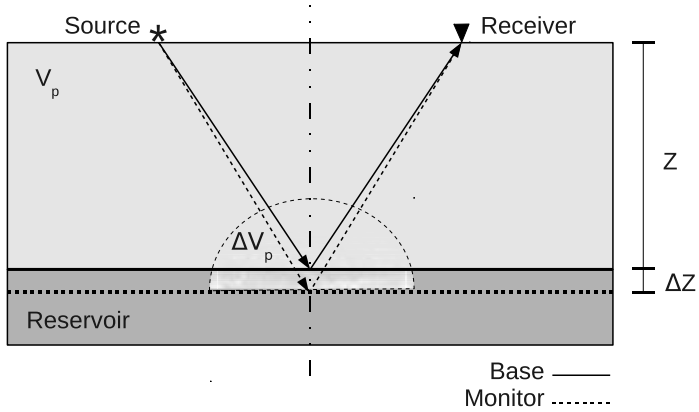

Figure 2.9: Empirical model linking seismic changes to overburden redistribution.

change in ground elevation, Δg_{def} is the change in gravity due to subsurface deformation, and Δg_{wt} is the change in gravity due to change in hight of the groundwater-table.

The first term, Δg_{res}, can be estimated using a forward model that includes reservoir modelling. The second term of Eq. 2.33, known as free air correction, can be approximated on land as:

$$\Delta g_{FA,l} = 3.086 \ \mu\text{Gal/cm} \tag{2.34}$$

and in water as:

$$\Delta g_{FA,w} = 2.66 \ \mu\text{Gal/cm} \tag{2.35}$$

The term Δg_{def} takes into consideration the effect of the displacement of the rock in the subsurface, and the change in density due to the compressibility of the material. In order to estimate the amount of this term, a forward model that includes geomechanical modelling is required. This is one of the main objective of this thesis. The last term in Eq. 2.33 is only present in land gravity monitoring, and it can be approximated by (Battaglia et al., 2008):

$$\Delta g_{wt} = 2\pi \cdot \mathcal{G} \cdot \rho_w \cdot \phi \cdot \Delta z \tag{2.36}$$

where $\mathcal{G}$ is the gravitational constant, ϕ is the ground porosity, ρ_w is the water density, and Δz is the change in depth of the groundwater-table.

By subtracting the the last three terms from the observed gravity change, an estimate of the change at the reservoir level is possible. The terms Δg_{FA} and Δg_{wt} can be monitored directly, but not the term Δg_{def}. The consequence is that a forward modelling is needed to get an estimated value to be subtracted from the observation.

Numerical modelling of gravity The calculation of the gravity potential of the Earth is often performed dividing the subsurface in element volumes, computing the volume integral, and, finally, summing the gravity contribution of each element volume.

The simplest approach to evaluate the integral of the Newton's law, is using the point-mass approximation. The subsurface is discretized in element volumes of the same size. The gravity potential is evaluated for each volume, assuming that the mass of the volume is concentrated at the centre of mass of the volume:

$$g = \mathcal{G} \cdot \rho \frac{V}{r_c^2} \tag{2.37}$$

where r_c is the distance of the centre of mass of the volume V from the observation point. The total gravity potential is the sum of the contribution of each element volume.

The advantage of the point mass approximation is the low computational time needed for the computation of the gravity potential. On the other hand, there are restrictions on the validity of the expression Eq. 2.37 near the computation point.

The right rectangular parallelepiped approximation is a well know approach for solving the volume integral of the Newton's law (Nagy, 2000, 1966):

$$g\left(P_0\right) = \mathcal{G} \cdot \rho \int_{z_1}^{z_2} \int_{y_1}^{y_2} \int_{x_1}^{x_2} \frac{dx \cdot dy \cdot dz}{r} \tag{2.38}$$

where $\mathcal{G}$ is the gravitational constant, P_0 is the observation point, x_1, x_2, y_1, y_2, z_1,and z_2 represent the coordinates of the corners of the rectangular prism, and r is the distance $\sqrt{x^2+y^2+z^2}$. A sketch of the rectangular parallelepiped is provided in Fig. 2.10. Eq. 2.38 can be approximated in the following way:

$$\begin{aligned} g\left(P_0\right) = \mathcal{G} \cdot \Big|\Big|\Big| & xy \ln\left(z+r\right) + yz \ln\left(x+r\right) + zx \ln\left(y+r\right) \\ & - \frac{x^2}{2} \tan^{-1} \frac{yz}{xr} - \frac{y^2}{2} \tan^{-1} \frac{zx}{yr} - \frac{z^2}{2} \tan^{-1} \frac{xy}{zr} \Big|_{x_1}^{x_2} \Big|_{y_1}^{y_2} \Big|_{z_1}^{z_2} \end{aligned} \tag{2.39}$$

The vertical component of gravity can be approximated in the following form:

$$g_z\left(P_0\right) = \mathcal{G} \cdot \Big|\Big|\Big| x \ln\left(y+r\right) + y \ln\left(x+r\right) - z \tan^{-1} \frac{xy}{zr} \Big|_{x_1}^{x_2} \Big|_{y_1}^{y_2} \Big|_{z_1}^{z_2} \tag{2.40}$$

The advantage of Nagy's approximation is that it is valid on the whole domain of integration, outside of or on the boundary of the prism. On the other hand,

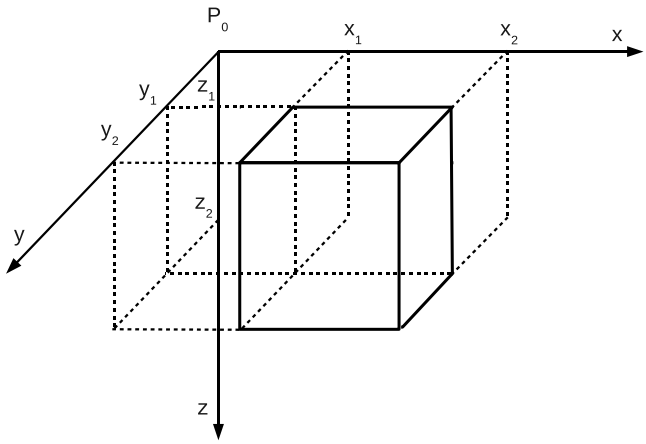

Figure 2.10: Sketch of the rectangular parallelepiped.

the computational time needed to evaluate the integral is such that it may be infeasible to use this method for integrating big volumes or fine discretized volumes.

Nagi's approximation is one of the techniques used to benchmark the forward model presented for the estimation of 4D gravity. The forward model requires the estimation of deformation and density change from a geomechanical model as input of the gravity model. The gravity model gives as output the estimate of change in gravity due to reservoir compaction. Further discussion on the application of Nagi's approximation is presented in Chapter 5.

2.4 Summary

The literature review described how reservoir compaction is a phenomenon that is an object of attention of different disciplines. Rock mechanics aims to forecast the displacement field and stress distribution inside and outside the depleting reservoir. Rock physics focus on the relation between physical changes and rock property changes. Geophysical monitoring observes the Earth to capture the changes in the subsurface. The three disciplines cooperate together to optimize the knowledge of the reservoir and its changes. The works reviewed in this chapter are those that directly influenced my research.

Chapter 3

Improved solution of displacements due to a compacting reservoir over a rigid basement

Pamela Tempone[1], Erling Fjær [1,2], Martin Landrø[1]

Published in the November 2010 issue of *Applied Mathematical Modelling*.

3.1 Abstract

Geertsma's analytical method is often used to compute strain and stress changes around a compacting geological reservoir. The present work extends Geertsma's solution by adding a rigid layer beneath the compacting reservoir. Analytical formulae are presented for all the components of displacement of a point in the subsurface. Our derivation includes the correction of an error found in the paper written by Sharma in 1956.

[1]Norwegian University of Science and Technology,
Department of Petroleum Engineering and Applied Geophysics,
S.P.Andersens vei 15A, N-7491 Trondheim, Norway
[2]SINTEF Petroleum Research,
S.P. Andersens vei 15 B, NO-7031 Trondheim, Norway

3.2 Introduction

Reservoir compaction due to hydrocarbon production causes changes in displacement, stress and strain fields in the subsurface. The propagation of the compaction to the surface may result in visible subsidence and changes in the seismic response. Some examples of compacting reservoirs are the Valhall field (Barkved and Kristiansen, 2005), the Shearwater field (Staples et al., 2007), and the Dan field (Hatchell et al., 2007), all located in the North Sea. Forward models for predicting geomechanical changes due to pressure depletion are of interest for monitoring subsidence, for estimating 4D seismic changes, and for understanding the potential of induced seismicity.

Various authors have studied the effects of hydrocarbon production on subsidence or displacement, strain and stress fields. In the group of the analytical methods, Geertsma is one of the most cited. In 1973, Geertsma (Geertsma, 1973a) proposed a solution for displacements and stresses based on the theory of poro-elasticity. He used as basis for his formulation the concept of nucleus of strain in analogy with the theory of thermo-elasticity (Nowacki, 1986; Goodier, 1937; Mindlin and Cheng, 1950). His model consists of a circular compacting reservoir buried in a homogeneous and linear elastic half space. In 1974, van Opstal (van Opstal, 1974) studied the vertical displacement at the free surface adding a rigid basement to Geertsma's model. Later, Fokker and Orlic (Fokker and Orlic, 2006) proposed a semi-analytical model for the prediction of subsidence in a multi-layered visco-elastic subsurface.

The alternative to the analytical solution is the use of numerical codes, based for instance on finite element methods. One method is explicit coupling, where changes in the pore-pressure coming from a conventional fluid simulator induce changes in stresses and strains in the geomechanical code (Minkoff et al., 1999). Another one is the full coupling of flow simulation and geomechanical modeling, as proposed by Settari in 2001 (Settari and Walters, 2001). These methods are more flexible with respect to geometry and heterogeneity of the subsurface, material constitutive behaviour, fluid properties and flow behaviour; however, the complexity of the models cause an increase in the time needed for the construction and the computation.

The present paper extends Geertsma's solution to the case of a compacting reservoir over a rigid basement. The method proposed here stresses the link between the presence of a rigid basement and its consequences on the displacement field created by the compacting reservoir. The rigid basement, for example, could represent crystalline basement rocks underlying a sedimentary basin; or a relatively stiff carbonate sequence underlying a soft clastic sequence.

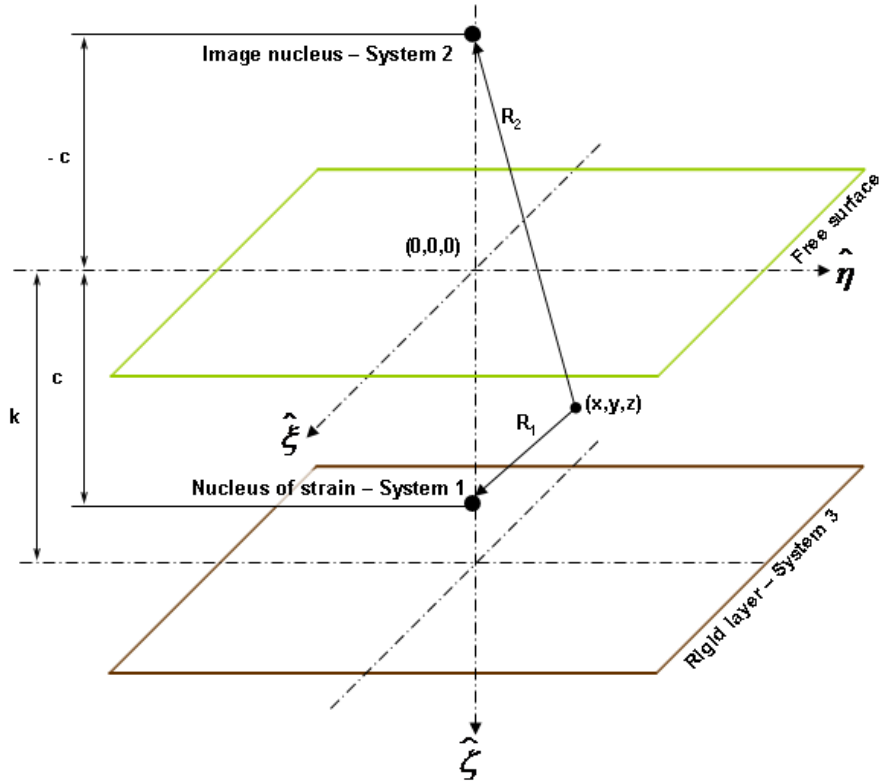

Figure 3.1: *Rigid basement sketch.* Sketch of the problem formulated for a nucleus of strain buried at depth c and lying over a hard basement.

The main objective is to create a tool which could easily be added to a code based on Geertsma's solution, and maintain the low computational effort. Formulae for all the components of displacement for a point buried in the half space are derived based on the derivation proposed by Sharma (Sharma and Pilani, 1956), who solved the analogous thermal problem. Here, we repeat his derivation, correct an error and derive the solutions for all three displacements components. The same path was followed by van Opstal (van Opstal, 1974) who, as noted above, derived an expression for the vertical displacement of the free surface.

3.3 Model and basic equations

The paper derives the analytical solution of the displacements due to a system consisting of a compacting reservoir and a rigid basement. As in Geertsma's model, the medium inside the reservoir and between the free surface and the rigid basement in linear elastic and has uniform and isotropic deformation properties. The displacement inside the basement is zero. We assume that production cause a uniform pore pressure change, Δp, within the reservoir, and none in the surroundings. The reservoir is discretized in N blocks of volume V each. The centre of each block represents the coordinate of a nucleus of poro-elastic strain, which causes a displacement field due to the pressure drop Δp. The sketch of the system solved for a single nucleus buried at depth c is represented in Fig. 3.1. In our system of reference, the positive side of the vertical axis is inside the ground. The summation of the displacement fields of all nuclei of the discretization gives the solution of the problem.

The derivation of the solution for the single nucleus is developed in three steps:

1. Firstly, the systems for stress and displacement are found for the poro-elastic nucleus in the infinite domain;
2. Then, the stresses acting through the free surface are nullified by superimposing a second system of stress due to an image nucleus at the point $(0, 0, -c)$. The sum of the two systems determines stress and displacement fields due to the nucleus in a semi-infinite domain;
3. Finally, a third system is found in such a way that keeps the surface at $z = 0$ free of stresses and satisfies the rigidity of the basement at $z = k$.

The problem has to be physically possible in an elastic solid, thus the consistency equations and the equilibrium equations have to be satisfied by each system s. Following the method proposed by Sharma (Sharma and Pilani, 1956), our problem must satisfy Beltrami's equations (Beltrami, 1902):

$$\begin{cases} \widehat{xz}_s = -\dfrac{z}{2\,(1+\nu)}\dfrac{\partial \theta_s}{\partial x} + \psi_{s1} \\ \widehat{yz}_s = -\dfrac{z}{2\,(1+\nu)}\dfrac{\partial \theta_s}{\partial y} + \psi_{s2} \\ \widehat{zz}_s = -\dfrac{z}{2\,(1+\nu)}\dfrac{\partial \theta_s}{\partial z} + \psi_{s3} \end{cases} \tag{3.1}$$

the equations of equilibrium:

$$\frac{\partial \theta_s}{\partial z} = 2\,(1+\,\nu)\,\left\{\frac{\partial \psi_{s1}}{\partial x} + \frac{\partial \psi_{s2}}{\partial y} + \frac{\partial \psi_{s3}}{\partial z}\right\} \tag{3.2}$$

and the generalized Hooke's law for an elastic medium:

$$\begin{cases} \dfrac{\partial u_s}{\partial z} = \dfrac{1}{E}[(1+\,\nu)\,\widehat{zz}_s - \nu\,\theta_s] \\ \dfrac{\partial v_s}{\partial z} + \dfrac{\partial u_s}{\partial y} = \dfrac{2\,(1+\,\nu)}{E}\,\widehat{yz}_s \\ \dfrac{\partial w_s}{\partial z} + \dfrac{\partial u_s}{\partial x} = \dfrac{2\,(1+\,\nu)}{E}\,\widehat{xz}_s \end{cases} \tag{3.3}$$

where u, v, w are the displacement components, $\widehat{xz}_s, \widehat{yz}_s, \widehat{zz}_s$ are the stress components, $\theta_{\mathbf{s}}$ is the first stress invariant,ψ_{s1}, ψ_{s2}, ψ_{s3} are harmonic functions (see Goodier (1937) and Nowacki (1986) for the definition of these functions). E and ν are Young's modulus and Poisson's ratio of the drained framework of the material between the free surface and the rigid basement.

3.4 Solution of the problem

3.4.1 System 1 – Nucleus of strain in the infinite space

The first step of the derivation is to define the displacement field due to the nucleus in the infinite space. Considering that the medium of the model is poro-elastic, we can apply the displacement potential formulated by Geertsma through the following equation:

$$\Phi = -\frac{C_m\,V\,\Delta p}{4\,\pi\,R_1} \tag{3.4}$$

where $R_1 = \sqrt{x^2+y^2+(z-c)^2}$ is the distance from the point (x, y, z) to the nucleus, V is the volume of the nucleus, and Δp is the pressure drop. C_m is the uniaxial compaction coefficient defined as (Geertsma, 1966):

$$C_m = \frac{1}{E}\cdot\frac{(1+\nu)\cdot(1-2\nu)}{1-\nu} \tag{3.5}$$

The gradient of Eq. (3.4) gives the solution for the displacements:

$$\begin{cases} w_1 = \dfrac{\partial \Phi}{\partial x} = \dfrac{A_g\,(1+\nu)}{E}\dfrac{\partial V_1}{\partial x} = \\ \quad = \dfrac{A_g\,(1+\nu)}{E}\displaystyle\int_0^\infty \left[\mathrm{e}^{\lambda\,\varepsilon(z-c)}\dfrac{\partial \mathrm{J}_0\,(\lambda\,r)}{\partial x}\right] d\lambda \\ \\ v_1 = \dfrac{\partial \Phi}{\partial y} = \dfrac{A_g\,(1+\nu)}{E}\dfrac{\partial V_1}{\partial y} = \\ \quad = \dfrac{A_g\,(1+\nu)}{E}\displaystyle\int_0^\infty \left[\mathrm{e}^{\lambda\,\varepsilon(z-c)}\dfrac{\partial \mathrm{J}_0\,(\lambda\,r)}{\partial y}\right] d\lambda \\ \\ u_1 = \dfrac{\partial \Phi}{\partial z} = \dfrac{A_g\,(1+\nu)}{E}\dfrac{\partial V_1}{\partial z} = \\ \quad = -\dfrac{A_g\,(1+\nu)}{E}\displaystyle\int_0^\infty \left[\lambda\,\varepsilon\,\mathrm{e}^{\lambda\,\varepsilon(z-c)}\mathrm{J}_0\,(\lambda\,r)\right] d\lambda \end{cases} \tag{3.6}$$

where

$$r = \sqrt{x^2+y^2} \tag{3.7}$$

$$\varepsilon = \begin{cases} -1 & \text{if } z > c \\ +1 & \text{if } z < c \end{cases} \tag{3.8}$$

$$A_g = -\frac{C_m\,V\,E\,\Delta p}{4\,\pi\,(1+\nu)} \tag{3.9}$$

and where the following formulation is used as an alternative and convenient way of expressing the singularity $\dfrac{1}{R_1}$:

$$V_1 = \frac{1}{R_1} = \int_0^\infty \mathrm{e}^{-\lambda\varepsilon(z-c)}\mathrm{J}_0\,(\lambda\,r)\,d\lambda \tag{3.10}$$

Later on, indeed, it will be shown that this Bessel function is common for all the systems, and will cancel while solving the last system of linear equations.

Given the displacement of Eq. (3.6), the stresses can be calculated as follows:

$$\begin{cases} \widehat{xz}_1 = A_g \dfrac{\partial^2 V_1}{\partial x \partial z} = -A_g \displaystyle\int_0^\infty \lambda \, \mathrm{e}^{-\lambda \varepsilon (z-c)} \frac{\partial \mathrm{J}_0 (\lambda r)}{\partial x} d\lambda \\ \widehat{yz}_1 = A_g \dfrac{\partial^2 V_1}{\partial y \partial z} = -A_g \displaystyle\int_0^\infty \lambda \, \mathrm{e}^{-\lambda \varepsilon (z-c)} \frac{\partial \mathrm{J}_0 (\lambda r)}{\partial y} d\lambda \\ \widehat{zz}_1 = A_g \dfrac{\partial^2 V_1}{\partial z^2} = A_g \displaystyle\int_0^\infty \lambda^2 \, \mathrm{e}^{-\lambda \varepsilon (z-c)} \mathrm{J}_0 (\lambda r) d\lambda \end{cases} \tag{3.11}$$

3.4.2 System 2 – Image nucleus

In order to find displacement and stress fields of the nucleus buried in the half space, we need to add the effect of an image nucleus positioned in such a way that the sum of System 1 and System 2 satisfies the boundary conditions at the free surface:

$$\widehat{xz}_1 + \widehat{xz}_2 = \widehat{yz}_1 + \widehat{yz}_2 = \widehat{zz}_1 + \widehat{zz}_2 = 0, \qquad \text{at} \quad z = 0 \tag{3.12}$$

This is fulfilled if:

$$\begin{cases} \psi_{21} = A_g \dfrac{\partial^2 V_2}{\partial x \partial z} \\ \psi_{22} = A_g \dfrac{\partial^2 V_2}{\partial y \partial z} \\ \psi_{23} = -A_g \dfrac{\partial^2 V_2}{\partial z^2} \end{cases} \tag{3.13}$$

where

$$V_2 = \frac{1}{R_2} = \int_0^\infty \mathrm{e}^{-\lambda (z+c)} \mathrm{J}_0 (\lambda r) \, d\lambda \tag{3.14}$$

and $R_2 = \sqrt{x^2 + y^2 + (z+c)^2}$, that is the distance from the point (x, y, z) to the image nucleus. The formula for the first stress invariant is derived from Eq. (3.2):

$$\theta_2 = -4 A_g (1 + \nu) \frac{\partial^2 V_2}{\partial z^2} \tag{3.15}$$

Then, substituting this value in Eq. (3.1), we find the formulae for the stresses in the second system:

$$\begin{cases} \widehat{xz}_2 = 2\,A_g\,z\,\dfrac{\partial^3 V_2}{\partial x \partial z^2} - A_g\,\dfrac{\partial^2 V_2}{\partial x \partial z} \\ \\ \widehat{yz}_2 = 2\,A_g\,z\,\dfrac{\partial^3 V_2}{\partial y \partial z^2} - A_g\,\dfrac{\partial^2 V_2}{\partial y \partial z} \\ \\ \widehat{zz}_2 = 2\,A_g\,z\,\dfrac{\partial^3 V_2}{\partial z^3} - A_g\,\dfrac{\partial^2 V_2}{\partial z^2} \end{cases} \tag{3.16}$$

Writing Eq. (3.17) in terms of Bessel functions, we have:

$$\begin{cases} \widehat{xz}_2 = A_g \displaystyle\int_0^\infty [2\,z\,\lambda - 1]\,\lambda\,\mathrm{e}^{-\lambda(z+c)}\frac{\partial \mathrm{J}_0\,(\lambda\,r)}{\partial x}\,d\lambda \\ \\ \widehat{yz}_2 = A_g \displaystyle\int_0^\infty [2\,z\,\lambda - 1]\,\lambda\,\mathrm{e}^{-\lambda(z+c)}\frac{\partial \mathrm{J}_0\,(\lambda\,r)}{\partial y}\,d\lambda \\ \\ \widehat{zz}_2 = -A_g \displaystyle\int_0^\infty [2\,z\,\lambda + 1]\,\lambda^2\,\mathrm{e}^{-\lambda(z+c)}\mathrm{J}_0\,(\lambda\,r)\,d\lambda \end{cases} \tag{3.17}$$

The derivation of the displacement is now possible. For the vertical component, we first need to substitute Eq. (3.15) and the third line of Eq. (3.17) into the first line of Eq. (3.3):

$$\frac{\partial u_2}{\partial z} = \frac{A_g\,(1+\,\nu)}{E}\,\left\{2\,z\,\frac{\partial^3 V_2}{\partial z^3} - (3-4\,\nu)\frac{\partial^2 V_2}{\partial z^2}\right\} \tag{3.18}$$

Then, integrating over z and simplifying, we obtain the vertical displacement as follow:

$$u_2 = \frac{A_s\,(1+\,\nu)}{E}\,\left\{2\,z\,\frac{\partial^2 V_2}{\partial z^2} - (3-4\,\nu)\frac{\partial V_2}{\partial z}\right\} \tag{3.19}$$

At this point, we observe that Eq. (3.19) differs from the formula derived by Sharma in 1956 (Sharma and Pilani, 1956). This discrepancy is due to an error in Sharma's derivation as mentioned by van Opstal in 1974 (van Opstal, 1974). Including this correction in the solution of the second and the third equation of system Eq. (3.3), we find the components of the displacement for

the second system:

$$\begin{cases} w_2 = A_g \dfrac{(1+\nu)}{E} \displaystyle\int_0^\infty [3 - 4\,\nu - 2\,z\,\lambda]\ \mathrm{e}^{-\lambda(z+c)} \frac{\partial \mathrm{J}_0(\lambda\, r)}{\partial x}\, d\lambda \\ v_2 = A_g \dfrac{(1+\nu)}{E} \displaystyle\int_0^\infty [3 - 4\,\nu - 2\,z\,\lambda]\ \mathrm{e}^{-\lambda(z+c)} \frac{\partial \mathrm{J}_0(\lambda\, r)}{\partial y}\, d\lambda \\ u_2 = A_g \dfrac{(1+\nu)}{E} \displaystyle\int_0^\infty [3 - 4\,\nu + 2\,z\,\lambda]\,\lambda\, \mathrm{e}^{-\lambda(z+c)} \mathrm{J}_0(\lambda\, r)\, d\lambda \end{cases} \tag{3.20}$$

3.4.3 System $1+2$ – Nucleus of strain in the half space

Stresses and displacements for the nucleus of strain buried in the half space come from the sum of the solution of the previous two systems. Hence the stresses are:

$$\begin{cases} \widehat{xz}_1 + \widehat{xz}_2 = A_g \displaystyle\int_0^\infty \lambda \left[\mathrm{e}^{-\lambda\,\varepsilon\,(z-c)} + (1 - 2\,z\,\lambda)\ \mathrm{e}^{-\lambda(z+c)}\right] \frac{\partial \mathrm{J}_0(\lambda\, r)}{\partial x}\, d\lambda \\ \widehat{yz}_1 + \widehat{yz}_2 = A_g \displaystyle\int_0^\infty \lambda \left[\mathrm{e}^{-\lambda\,\varepsilon\,(z-c)} + (1 - 2\,z\,\lambda)\ \mathrm{e}^{-\lambda(z+c)}\right] \frac{\partial \mathrm{J}_0(\lambda\, r)}{\partial y}\, d\lambda \\ \widehat{zz}_1 + \widehat{zz}_2 = -A_g \displaystyle\int_0^\infty \lambda^2 \left[\mathrm{e}^{-\lambda\,\varepsilon\,(z-c)} - (1 + 2\,z\,\lambda)\ \mathrm{e}^{-\lambda(z+c)}\right] \mathrm{J}_0(\lambda\, r)\, d\lambda \end{cases} \tag{3.21}$$

and the displacements are:

$$\begin{cases} w_1 + w_2 = \\ A_g \dfrac{(1+\nu)}{E} \displaystyle\int_0^\infty \left[\mathrm{e}^{\lambda\,\varepsilon\,(z-c)} + (3 - 4\,\nu - 2\,z\,\lambda)\ \mathrm{e}^{-\lambda(z+c)}\right] \frac{\partial \mathrm{J}_0(\lambda\, r)}{\partial x}\, d\lambda \\ v_1 + v_2 = \\ A_g \dfrac{(1+\nu)}{E} \displaystyle\int_0^\infty \left[\mathrm{e}^{\lambda\,\varepsilon\,(z-c)} + (3 - 4\,\nu - 2\,z\,\lambda)\ \mathrm{e}^{-\lambda(z+c)}\right] \frac{\partial \mathrm{J}_0(\lambda\, r)}{\partial y}\, d\lambda \\ u_1 + u_2 = \\ -A_g \dfrac{(1+\nu)}{E} \displaystyle\int_0^\infty \lambda\ \left[\varepsilon\, \mathrm{e}^{\lambda\,\varepsilon\,(z-c)} + (3 - 4\,\nu + 2\,z\,\lambda)\ \mathrm{e}^{-\lambda(z+c)}\right] \mathrm{J}_0(\lambda\, r)\, d\lambda \end{cases} \tag{3.22}$$

The solution proposed here for the displacements, Eq. (3.22), is consistent with the one derived by Geertsma in 1973. The only difference is the way the singularity is expressed mathematically.

3.4.4 System 3 – Rigid basement

The next step is finding the solution for the system that accounts for the effects of the rigid basement. As proposed by Sharma (Sharma and Pilani, 1956), we can express the Eq. (3.1) in the following form:

$$\begin{cases} \widehat{xz}_3 = -\dfrac{z}{2\,(1+\,\nu)}\dfrac{\partial\theta_3}{\partial x}\displaystyle\int_0^\infty B\,\sinh(z\lambda)\,\frac{\partial \mathrm{J}_0\,(\lambda\,r)}{\partial x}\,d\lambda \\ \widehat{yz}_3 = -\dfrac{z}{2\,(1+\,\nu)}\dfrac{\partial\theta_3}{\partial y}\displaystyle\int_0^\infty B\,\sinh(z\lambda)\,\frac{\partial \mathrm{J}_0\,(\lambda\,r)}{\partial y}\,d\lambda \\ \widehat{zz}_3 = -\dfrac{z}{2\,(1+\,\nu)}\dfrac{\partial\theta_3}{\partial z}\displaystyle\int_0^\infty C\,\sinh(z\lambda)\,\mathrm{J}_0\,(\lambda\,r)\,d\lambda \end{cases} \tag{3.23}$$

where B and C are unknown functions of λ. Written in this form, the stresses of the third system are zero at $z = 0$; thus we shall now define B and C such that the displacement at the basement vanishes.
From Eq. (3.2), the first stress invariant for the third system becomes:

$$\theta_3 = 2\,(1+\,\nu)\int_0^\infty \lambda\,[C\,\cosh(z\lambda) - B\,\sinh(z\lambda)]\,\mathrm{J}_0\,(\lambda\,r)\,d\lambda \tag{3.24}$$

and substituting Eq. (3.24) in Eq. (3.23), we can write the stresses as follow:

$$\begin{cases} \widehat{xz}_3 = \\ \displaystyle\int_0^\infty \{-\lambda\,z\,[C\,\sinh(z\lambda) - B\,\cosh(z\lambda)] + B\,\sinh(z\lambda)\}\frac{\partial \mathrm{J}_0\,(\lambda\,r)}{\partial x}\,d\lambda \\ \widehat{yz}_3 = \\ \displaystyle\int_0^\infty \{-\lambda\,z\,[C\,\sinh(z\lambda) - B\,\cosh(z\lambda)] + B\,\sinh(z\lambda)\}\frac{\partial \mathrm{J}_0\,(\lambda\,r)}{\partial y}\,d\lambda \\ \widehat{zz}_3 = \\ \displaystyle\int_0^\infty \{-\lambda^2\,z\,[C\,\cosh(z\lambda) - B\,\sinh(z\lambda)] + \lambda\,C\,\sinh(z\lambda)\}\mathrm{J}_0\,(\lambda\,r)\,d\lambda \end{cases} \tag{3.25}$$

Then, using Eq. (3.3) again, we obtain the displacement of the third system:

$$\begin{cases} w_3 = & \dfrac{(1+\nu)}{E}\displaystyle\int_0^\infty \{\frac{B}{\lambda}\left[2\,(1-\nu)\,\cosh(z\lambda)+\lambda\,z\,\sinh(z\lambda)\right]- \\ & \dfrac{C}{\lambda}\left[(1-2\,\nu)\,\sinh(z\lambda)+\lambda\,z\,\cosh(z\lambda)\right]\}\,\dfrac{\partial \mathrm{J}_0(\lambda\,r)}{\partial x}\,d\lambda \\ v_3 = & \dfrac{(1+\nu)}{E}\displaystyle\int_0^\infty \{\frac{B}{\lambda}\left[2\,(1-\nu)\,\cosh(z\lambda)+\lambda\,z\,\sinh(z\lambda)\right]- \\ & \dfrac{C}{\lambda}\left[(1-2\,\nu)\,\sinh(z\lambda)+\lambda\,z\,\cosh(z\lambda)\right]\}\dfrac{\partial \mathrm{J}_0(\lambda\,r)}{\partial y}\,d\lambda \\ u_3 = & \dfrac{(1+\nu)}{E}\displaystyle\int_0^\infty \{B\left[\lambda\,z\,\cosh(z\lambda)-(1-2\,\nu)\,\sinh(z\lambda)\right]+ \\ & C\left[2\,(1-\nu)\cosh(z\lambda)-\lambda\,z\,\sinh(z\lambda)\right]\}\mathrm{J}_0(\lambda\,r)\,d\lambda \end{cases} \tag{3.26}$$

Now, the functions B and C can be determined imposing the boundary conditions of the rigid plane:

$$u_1+u_2+u_3=v_1+v_2+v_3=w_1+w_2+w_3=0, \qquad \text{at} \quad z=k \tag{3.27}$$

that are verified if:

$$B=\frac{1}{\Delta}\{\lambda\,L\left[2\,(1-\nu)\cosh(k\lambda)-\lambda\,k\,\sinh(k\lambda)\right]+ \lambda\,M\left[(1-2\,\nu)\,\sinh(k\lambda)+\lambda\,k\,\cosh(k\lambda)\right]\} \tag{3.28}$$

$$C=\frac{1}{\Delta}\{\lambda\,L\left[(1-2\,\nu)\sinh(k\lambda)-\lambda\,k\,\cosh(k\lambda)\right]+ \lambda\,M\left[2\,(1-\nu)\,\cosh(k\lambda)+\lambda\,k\,\sinh(k\lambda)\right]\} \tag{3.29}$$

where

$$L=A_g\left[(4\,\nu-3+2\,k\lambda)\,\mathrm{e}^{-\lambda\,(k+c)}-\mathrm{e}^{\lambda\,\varepsilon\,(k-c)}\right] \tag{3.30}$$

$$M=A_g\left[(4\,\nu-3-2\,k\lambda)\,\mathrm{e}^{-\lambda\,(k+c)}-\varepsilon\,\mathrm{e}^{\lambda\,\varepsilon\,(k-c)}\right] \tag{3.31}$$

$$\Delta=(4\,\nu-3)\cosh^2(k\lambda)-k^2\lambda^2-(1-2\,\nu)^2 \tag{3.32}$$

3.4.5 System $1+2+3$ – Nucleus of strain over a rigid basement

Finally, the solution for a poro-elastic nucleus of strain over a rigid basement is the resultant of the three systems previously solved. Hence the components

for the displacement are:

$$\begin{cases} u_t = u_1 + u_2 + u_3 \\ v_t = v_1 + v_2 + v_3 \\ w_t = w_1 + w_2 + w_3 \end{cases} \tag{3.33}$$

The impact of the rigid basement is illustrated in Fig. 3.2(b), showing the vertical displacement above and below a single shrinking nucleus, both for the Rigid Basement model (System $1+2+3$), the Geertsma model (System $1+2$) and the basement correction (System 3). The nucleus is sitting at 800 m depth and the rigid basement is at 1000 m depth. The nucleus is 100 m thick and it has a base area of 1100 m^2. The results are due to a pressure depletion of 10 MPa. The uniaxial compaction coefficient is $2.5{\cdot}10^{-4}$ MPa^{-1}, and the Poisson's ratio is 0.25.

In the overburden, the presence of the rigid basement is seen to induce a larger downwards movement, i.e. larger subsidence. In the underburden, the vertical displacement is vanishing at the rigid basement, hence the displacement is less than predicted by the Geertsma model. Note that System $1+2$ and System $1+2+3$ are only valid outside the nucleus, therefore the curves are truncated at the boundary of the nucleus. Since the displacements are proportional to the product of the volume of the nucleus times the pressure drop (see Eq. 3.9), we will get the same displacement outside the nucleus if the volume of the nucleus is reduced by a given factor and the pressure drop is increased by the same factor.

3.5 Extension to arbitrary reservoir shape

The displacement due to the compaction of an arbitrary shaped reservoir can be found by dividing the reservoir into an arbitrary number of volumes and assuming a nucleus of poro-elastic strain into each volume. As addressed by Geertsma and Van Opstal (1973) and Lewis et al. (Lewis et al., 1983), special care is needed in choosing the number of discretization volumes, which is geometry dependent. The displacement can then be found by summation as follow:

$$\begin{cases} U_{res}(x,y,z) = \sum_{i=1}^{N} u_{t,i}(x,y,z) \\ V_{res}(x,y,z) = \sum_{i=1}^{N} v_{t,i}(x,y,z) \\ W_{res}(x,y,z) = \sum_{i=1}^{N} w_{t,i}(x,y,z) \end{cases} \tag{3.34}$$

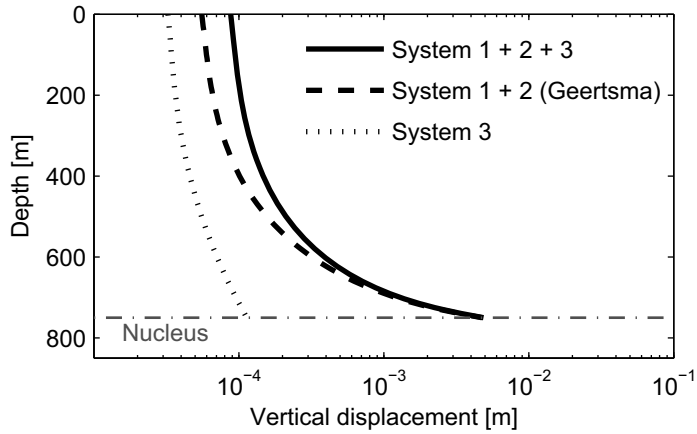

(a) Overburden – Log scale

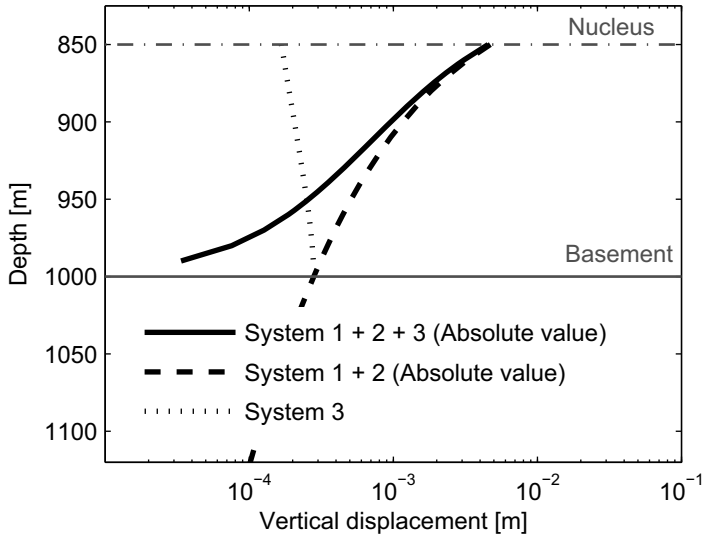

(b) Underburden – Log scale

Figure 3.2: ***a)*** *overburden and* ***b)*** *underburden displacement due to a single nucleus of strain.* Vertical displacement versus depth as predicted by the Rigid Basement model (System $1 + 2 + 3$), the Geertsma's model (System $1 + 2$) and the basement correction (System 3), due to a shrinking nucleus sitting at 800 m depth and a rigid basement at 1000 m depth. Note that the signs of the displacements for System $1 + 2 + 3$ and System $1 + 2$ have been changed in the underburden due to the logarithmic axis.

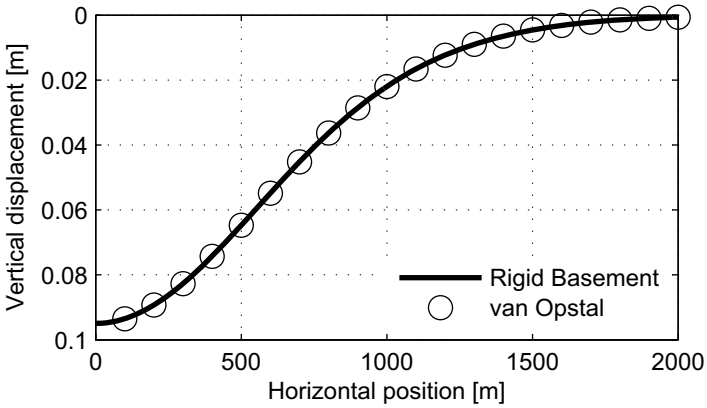

Figure 3.3: *Free surface subsidence.* Subsidence of the free surface computed using both van Opstal's solution and Rigid Basement solution.

The strain components can be found numerically as:

$$\varepsilon_{ij} = \frac{1}{2}\left(\frac{\Delta U_{res,i}}{\Delta x_j} + \frac{\Delta U_{res,j}}{\Delta x_i}\right) \tag{3.35}$$

and, from Hooke's law, the stresses:

$$\sigma_{ij} = \frac{E}{1+\nu}\left[\varepsilon_{ij} + \frac{\nu}{1-2\,\nu}\varepsilon\,\delta_{ij}\right] \tag{3.36}$$

where ε is the volumetric strain and δ_{ij} is the Kronecker delta.

The solution provided by these models is only valid outside the reservoir. In order to get an indication of what is happening inside the reservoir, we take linear interpolations of the displacements at the boundaries of the reservoir to represent the displacements inside the reservoir. This implies that the deformation of the reservoir is assumed to be uniform in the vertical direction. Note that our analyses in the following are focused on the rock around the reservoir, and that the stresses, strains and displacements shown inside the reservoir are only estimates based on this assumption.

The same method of summation and interpolation has been used in the next section to compute the solutions for Geertsma's model, that is for the case of a reservoir buried in a semi-infinite space (see Section 3.4.3).

3.6 Results

The presented method has been used to compare displacements, stresses and strains due to a compacting reservoir with and without rigid basement. As already stated, the solution of the case without the basement coincide with the solution proposed by Geertsma.

The reservoir analysed in this section is a cylinder with a vertical axis, with a radius of 500 m and a length of 100 m. It is positioned at a depth of 800 m, and, when present, the rigid basement is 150 m under the bottom of the reservoir. All results are due to a pressure depletion of 10 MPa. The uniaxial compaction coefficient is $2.5{\cdot}10^{-4}$ MPa^{-1}, and Poisson's ratio is 0.25. Each nucleus is 100 m thick and it has a base area of 1100 m^2, for a total of 715 nuclei. We define the vertical axis as positive downwards, thus downward movement is positive and uplift is negative. Stretching and tension are positive, while compaction and compression are negative.

The number of nuclei has been chosen such to be sufficiently high to give satisfying errors in displacement and strain, and to reduce the computational time. The source of the errors is the mathematical representation of the nucleus of strain, that is discontinuous at the centre of the nucleus. The errors are mainly localized close to the reservoir horizontal plan of symmetry of the reservoir, where the nucleus centres are positioned. The choice of the number of nuclei is arbitrary, and it depends on the accuracy required from the problem formulation. In our example, the error of the subsidence values found using the analytical solution by van Opstal (1974) and the semi-analytical solution presented in Section 3.5 is about 0.01 %.

In order to assess the correctness of the previous derivation, we benchmarked our method against the derivation for the displacement at the free surface found by van Opstal (van Opstal, 1974). As shown in Fig. 3.3, the subsidence of the free surface found using the two methods coincides; thus we assume that our derivation and results are valid.

Fig. 3.4 compares the results for free surface subsidence and vertical displacement of the top and bottom of the reservoir for Geertsma's and the Rigid Basement models. We observe that the free surface displacement is larger with a rigid basement than without; this is expected since the rigid basement will act as force keeping all movements downwards. The rigid basement also imposes an additional positive displacement to the top and bottom of the reservoir. Furthermore we observe that the deformed area at the free surface is larger than the deformed area of the top of the reservoir.

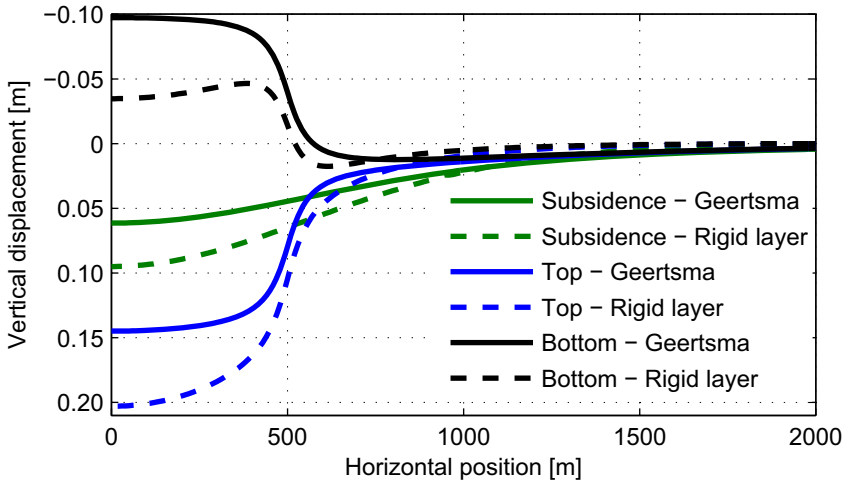

Figure 3.4: *Vertical movement of the layers.* Subsidence and vertical displacement of top and bottom of the reservoir due to pressure depletion ΔP with (Rigid Basement) and without (Geertsma) the effects of the rigid basement. According to our system of reference, the displacement is positive downwards.

The results for displacement, strain and stress are presented as 2D contour plots in Fig. 3.5(d) - Fig. 3.6(d). Both solutions are gathered in the same plot: Geertsma is on the right side and Rigid Basement is on the left side. In general, we observe an increase of the value of vertical displacement in the overburden and a decrease in the underburden. Looking at the radial displacements, we observe that the rocks of the overburden are pushed more toward the axis of symmetry when the rigid basement is present. On the other hand, the underburden moves less in the horizontal direction because the basement is closer. Moreover, vertical strain increases both in the overburden and in the underburden, while horizontal strain increases in the overburden and decreases in the underburden. This results in higher vertical stretching of the overburden and underburden, and higher horizontal compression of the overburden. The Rigid Basement model predicts a positive volumetric strain of the rock above and below the reservoir, while the Geertsma's model predicts almost no change in the volumetric strain around the reservoir. The values of the octahedral shear stress are higher in the overburden and lower in the underburden in the case with a rigid basement.

3.7 Conclusions

The present work extends Geertsma's model taking into account the effects of a rigid basement. The formulae derived for the three components of the displacement due to the presence of the basement can be easily implemented in a code based on Geertsma's solution, maintaining low computational efforts.

This simple analytical approach can serve as a help to understand and quickly evaluate the effect of introducing a more rigid basement close to a compacting reservoir. The more visible effects are the increase of subsidence and lowering of top reservoir, and the decrease of the uplift of bottom reservoir. Relevance should be also given to the increase of volumetric strain and stress in the underburden, which could be relevant for 4D seismic interpretation.

3.8 Acknowledgements

The authors acknowledge the Norwegian University of Science and Technology, the Norwegian Research Council and Total for sponsoring the presented work. The first author expresses her gratitude to her colleagues at the Department of Petroleum Engineering and Applied Geophysics for fruitful discussions.

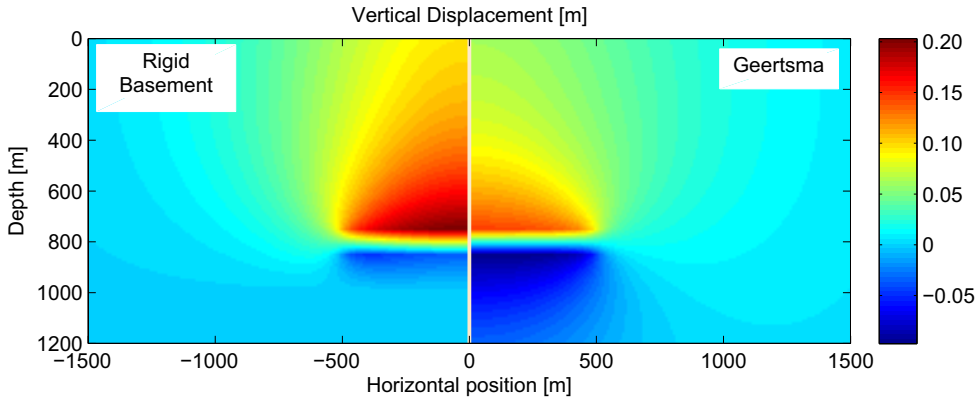

(a)

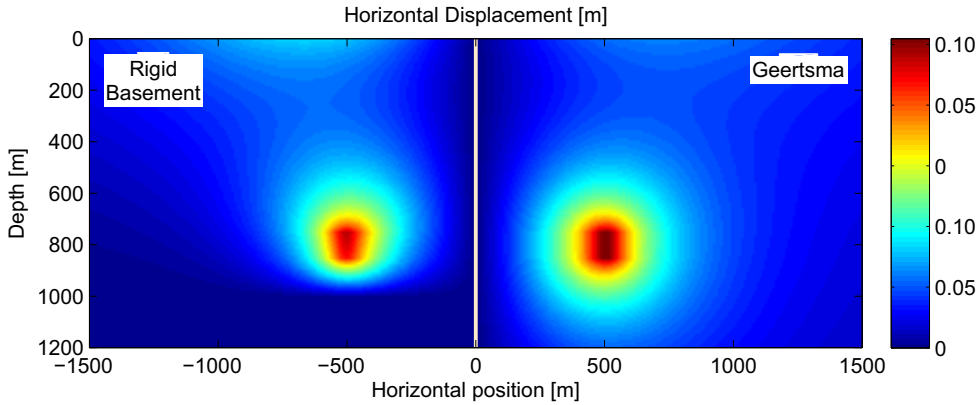

(b)

Figure 3.5: *Contour plot for displacement and strain.* Results for: **a)** vertical and **b)** horizontal displacement, **c)** vertical and **d)** horizontal strain. Each plot includes the results for the two models: Geertsma on the right side and Rigid Basement on the left side.

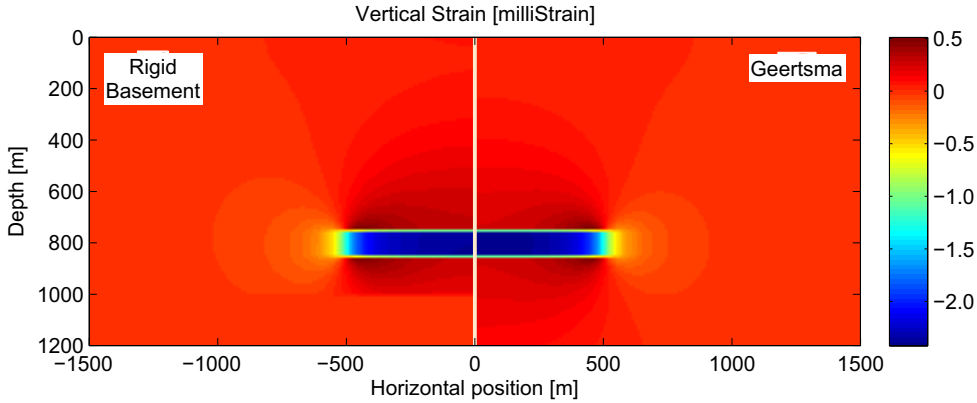

(c)

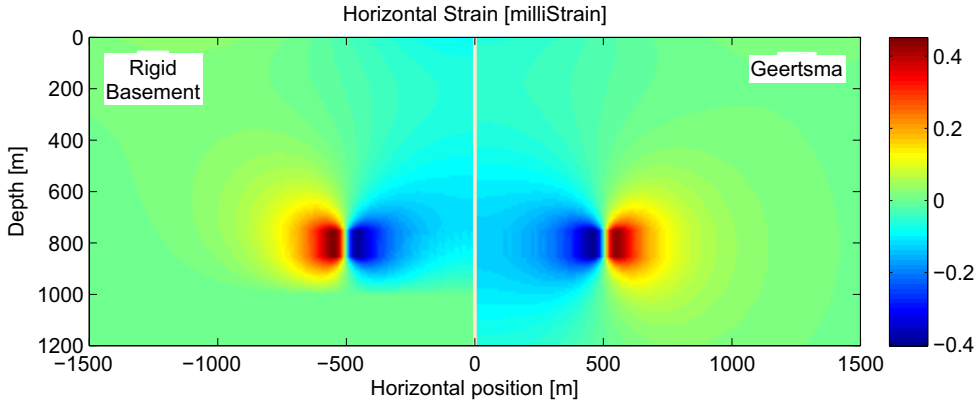

(d)

Figure 3.5: *Contour plot for displacement and strain.* Results for: **a)** vertical and **b)** horizontal displacement, **c)** vertical and **d)** horizontal strain. Each plot includes the results for the two models: Geertsma on the right side and Rigid Basement on the left side.

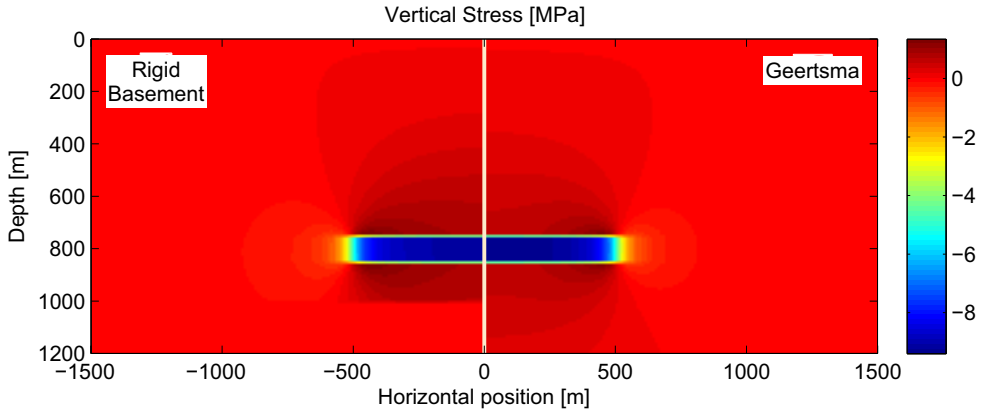

(a)

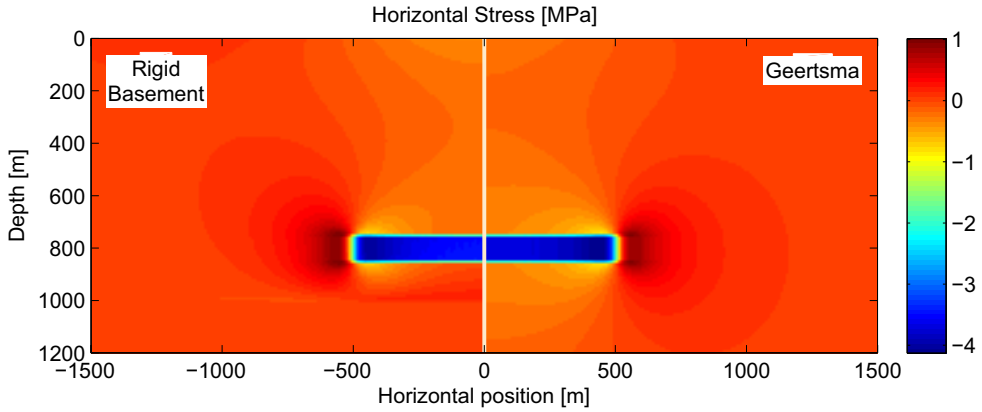

(b)

Figure 3.6: *Contour plot for stress and strain.* Results for: **a)** vertical and **b)** horizontal stress, **c)** volumetric strain, and **d)** octahedral shear stress. Each plot includes the results for the two models: Geertsma on the right side and Rigid Basement on the left side.

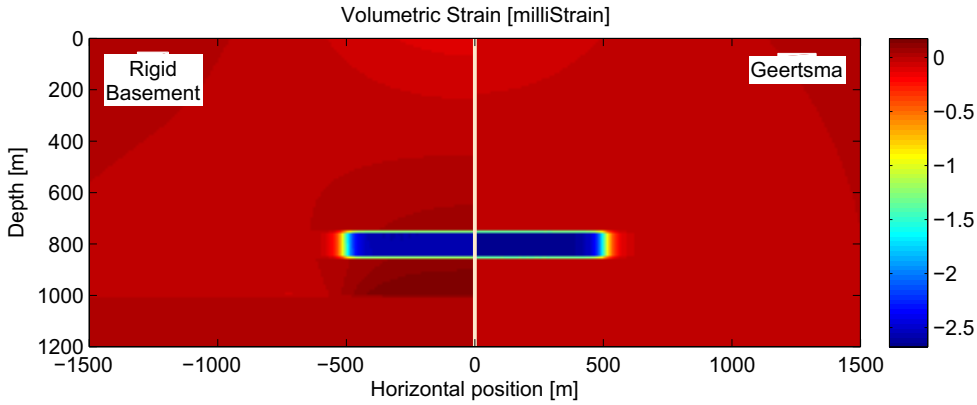

(c)

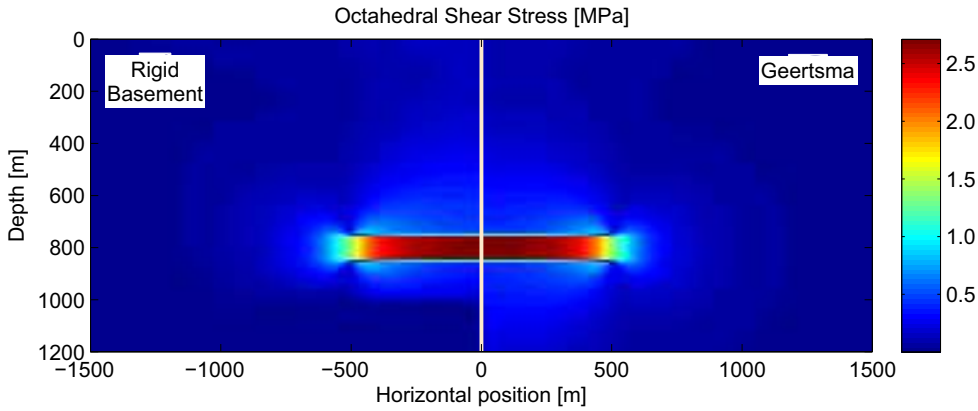

(d)

Figure 3.6: *Contour plot for stress and strain.* Results for: **a)** vertical and **b)** horizontal stress, **c)** volumetric strain, and **d)** octahedral shear stress. Each plot includes the results for the two models: Geertsma on the right side and Rigid Basement on the left side.

Chapter 4

Effects on time-lapse seismic of a hard rock layer beneath a compacting reservoir

Is not included due to copyright

Chapter 5

4D gravity response of compacting reservoirs

Is not included due to copyright

Chapter 6

Discussion

In the previous chapters, is has been demonstrated that the Rigid Basement model is a convenient tool to be used for feasibility studies on displacement and strain fields, and on 4D seismic and 4D gravity changes due to reservoir compaction. However, an interesting discussion arises when we consider the assumptions lying behind the model and its possible applications. This chapter contains a discussion on the limitation of the model, and a suggestion for further work on the model.

The assumption of linear elastic medium is generally accepted for the rocks faraway from the compacting reservoir. However, this may not be true near and inside the reservoir, where the rocks can behave plastically. In these areas, displacement and strain could be underestimated, causing a wrong estimation of 4D seismic and 4D gravity changes. Because of this observation, the two models can be considered as helpful tools for the prediction of the low frequency changes happening outside the reservoir, while alternative models may be considered inside the reservoir.

Furthermore, the rigid interface is the only heterogeneity considered by the model. Further changes of density and rock properties in vertical and horizontal directions are neglected, oversimplifying the geological section. The displacement and the strain, in this case, are underestimated in weaker layers and overestimated in harder layers. If a hard chalk layer is present in the overburden, for example, the displacement tends to disappear toward the layer and nullify inside and above the layer. Hence, subsidence and strain near the free surface would be negligible, and 4D gravity changes due to subsurface displacement would decrease substantially.

Another important heterogeneity of the subsurface is represented by reactivated faults. This event is possible when the faults fall into an area of strong

shear stress caused by reservoir compaction and redistribution of the subsurface. The reactivation adds a further stress field around the fault plane, that can affect 4D seismic and 4D gravity depending on the magnitude of the displacement and strain field generated.

The medium between the rigid layer and the surface is also considered to be isotropic. However, the depositional history of the sediments and the shapes of the grains are generally creating anisotropy in the geomechanical and geophysical properties of the rocks. Shale, for example, has the maximum component of stiffness perpendicular to the clay bedding, causing smaller deformation in this direction.

The reservoir geometry studied in the research work is limited to the vertical cylinder and vertical elliptical cylinder. However, natural reservoirs have complex shapes and thickness, and reservoir formations and basements can be tilted. An arbitrary shape of the reservoir can be model by both models, thanks to the versatile additivity property of the nucleus of strain. Geertsma's model can be also easily implemented to represent tilted reservoirs. On the case of the Rigid Basement model, however, the analytical formulation may limit its use to the case of horizontal reservoir and basement, even if this limitation has not been proven.

The limitations of the Rigid Basement model can be overcome by using a more complex numerical model, like a Finite Element Method model, a Discrete Element Method model, or a combination of the two. The numerical modelling is able to cope with more details present in the real geological section. However it needs more time to set up the model and to obtain the results. The computational time needed often direct the decision to model a 2D model. When a 3D modelling is necessary, the machine used for the computation increases in size and cost.

The results coming from Chapter 5 suggest further interesting studies on the 4D gravity technique. A comparison of real 4D gravity data and the results coming from the 4D gravity forward model including the rigid basement model, would be an example. Such comparison would prove the sensitivity of the 4D gravity technique to subsurface rock redistribution due to reservoir compaction.

A comparison between 4D seismic modelling and real data could provide useful knowledge too. One of the main conclusions of Chapter 4, indeed, is that the fast decrease in vertical strain in the underburden causes the fast decrease in time-shift observed in some field of the North Sea. However, a structured comparison between modelled results and real data could provide further proof to this statement.

Another idea for further studies comes from the non-linear behaviour of 4D gravity change versus depth and radius of the reservoir above the rigid basement. This behaviour suggests that there are combinations of reservoir depths and radii that would provide maximum 4D gravity change. A wide sensitivity study on these parameters could provide a map showing where high 4D gravity changes are expected. Such a map may be a useful tool for reservoir management and 4D gravity risk assessment.

Chapter 7

Conclusions

The PhD research achieved successfully the objective initially stated. First, the formulae for displacement and stress of an arbitrary point of the subsurface are derived for the case of a compacting reservoir above a rigid basement. Second, the formulae for the Rigid Basement model are introduced into a forward model for prediction of 4D seismic time-shifts and 4D gravity changes. Third, the results coming from the Rigid Basement model are compared with those coming from the well known Geertsma's model.

The formulae of the Rigid Basement model introduce an heterogeneity to Geertsma's model. The model clearly demonstrates the impact of heterogeneity in rock stiffness on geomechanical modeling, keeping low the number of the parameters needed for the estimation of the displacement. The use of the Rigid Basement model, indeed, resulted very handy and computationally fast during the sensitivity study presented in Chapter 5. This characteristic makes the RB model a convenient geomechanical model to be introduced in feasibility studies of compacting reservoirs.

From 4D seismic point of view, the Rigid Basement model predicts a decrease in velocity of the rocks in the underburden. This observation may be the explanation of the decrease in time-shifts in the underburden observed in Shearwater field by Staples et al. (2007), and in the decrease in velocity in the underburden observed in Valhall field by Hossein Mehdizadeh (personal communication, 2010). Including the Rigid Basement model in a 4D seismic forward model, may be a useful tool for the interpretation of slow-down below a compacting reservoir.

The change of gravity due to the subsurface deformation predicted using the Rigid Basement model, results above the current intra survey accuracy of 3–5 μGal. This finding agrees with other studies carried out with numerical

modelling (Currenti et al., 2007); however, it goes against the often used assumption that subsurface deformation may be neglected. Because of the low number of parameters needed, the Rigid Basement model qualifies to be a very useful and handy geomechanical model for broadening the knowledge on the effect of the subsurface deformation on 4D gravity.

In conclusion, the work presented in the thesis is demonstrating the impact of heterogeneity in the rock stiffness, it is narrowing the gap between the well known Geertsma's analytical model and Nature, and it is giving a useful tool for 4D seismic interpretation and 4D gravity prediction.

References

Barkved, O. and T. Kristiansen, 2005, Seismic time-lapse effects and stress changes: Examples from a compacting reservoir: The Leading Edge, **24**, 1244.

Barkved, O. I., T. Kristiansen, and E. Fjær, 2005, The 4D seismic response of a compacting reservoir—examples from the valhall field, norway: SEG Technical Program Expanded Abstracts, **24**, 2508–2511.

Battaglia, M., J. Gottsmann, D. Carbone, and J. Fernández, 2008, 4D volcano gravimetry: Geophysics, **73**, WA3–WA18.

Bauer, A., C. Lehr, F. Korndorffer, A. van der Linden, J. Dudley, T. Addis, K. Love, and M. Myers, 2008, Stress and pore-pressure dependence of sound velocities in shales: Poroelastic effects in time-lapse seismic: SEG Technical Program Expanded Abstracts, **27**, 1630–1634.

Beltrami, E., 1902, Opere matematiche (Vols. 1-4): Milano.

Bonaccorso, A., S. Cianetti, C. Giunchi, E. Trasatti, M. Bonafede, and E. Boschi, 2005, Analytical and 3D numerical modelling of Mt. Etna (Italy) volcano inflation: Geophysical Journal International, **163**, 852–862.

Bonafede, M. and M. Mazzanti, 1998, Modelling gravity variations consistent with ground deformation in the campi flegrei caldera (italy): Journal of Volcanology and Geothermal Research, **81**, 137–157.

Budiansky, B. and R. J. O'connell, 1976, Elastic moduli of a cracked solid: International Journal of Solids and Structures, **12**, 81 – 97.

Calvert, R., 2005, Insights and methods for 4D reservoir monitoring and characterization: 2005 Distinguished Instructor Short Course: Society of Exploration Geophysicists.

Cayol, V. and F. H. Cornet, 1998, Effects of topography on the interpretation of the deformation field of prominent volcanoes – Application to Etna: Geophysical Research Letters, **25**, 1979–1982.

Chapman, D. S., E. Sahm, and P. Gettings, 2008, Monitoring aquifer recharge using repeated high-precision gravity measurements: A pilot study in South Weber, Utah: Geophysics, **73**, WA83–WA93.

Conington, J., 1882, The odes and carmen saeculare of Horace: George Bell and Sons.

Cox, B. and P. Hatchell, 2008, Straightening out lateral shifts in time-lapse seismic: First Break, 93.

Currenti, G., C. Del Negro, and G. Ganci, 2007, Modelling of ground deformation and gravity fields using finite element method: an application to Etna volcano: Geophysical Journal International, **169**, 775–786.

Davis, K., Y. Li, and M. Batzle, 2008, Time–lapse gravity monitoring: A systematic 4D approach with application to aquifer storage and recovery: Geophysics, **73**, WA61–WA69.

Dieterich, J. H. and R. W. Decker, 1975, Finite element modeling of surface deformation associated with volcanism: Journal of Geophysical Research – Solid Earth, **80**, 4095–4102.

Du, J., S. Brissenden, P. McGillivray, S. Bourne, P. Hofstra, W. Roadarmel, E. Davis, S. Wolhart, and C. Wright, 2005, Mapping fluid flow in a reservoir using tiltmeter-based surface-deformation measurements: Presented at the SPE Annual Technical Conference and Exhibition.

Eiken, O., I. Brevik, R. Arts, E. Lindeberg, and K. Fagervik, 2000, Seismic monitoring of CO2 injected into a marine aquifer: Expanded Abstracts, 1623–1626.

Eiken, O., T. Stenvold, M. Zumberge, H. Alnes, and G. Sasagawa, 2008, Gravimetric monitoring of gas production from the Troll field: Geophysics, **73**, WA149–WA154.

Ferguson, J. F., F. J. Klopping, T. Chen, J. E. Seibert, J. L. Hare, and J. L. Brady, 2008, The 4D microgravity method for waterflood surveillance: Part 3 – 4D absolute microgravity surveys at Prudhoe Bay, Alaska: Geophysics, **73**, WA163–WA171.

Fjær, E., 2006, Modeling the stress dependence of elastic wave velocities in soft rocks.: Presented at the Golden Rocks 2006, The 41st US Symposium on Rock Mechanics (USRMS).

Fjær, E., R. Holt, P. Horsrud, A. Raaen, and R. Risnes, 2008, Petroleum related rock mechanics, 2nd edition ed. Developments in petroleum science: Elsevier.

Fokker, P. and B. Orlic, 2006, Semi-analytic modelling of subsidence: Mathematical geology, **38**, 565–589.

Folch, A., J. Fernández, J. B. Rundle, and J. Martí, 2000, Ground deformation in a viscoelastic medium composed of a layer overlying a half–space: a comparison between point and extended sources: Geophysical Journal International, **140**, 37–50.

Fuck, R., A. Bakulin, and I. Tsvankin, 2009, Theory of traveltime shifts around compacting reservoirs: 3D solutions for heterogeneous anisotropic media: Geophysics, **74**, D25.

Gassmann, F., 1951, Elastic waves through a packing of spheres: Geophysics, **16**, 673.

Geertsma, J., 1957, The effect of fluid pressure decline on volumetric changes of porous rocks: Transactions of the American Institute of Mining, Metallurgical and Petroleum Engineers, **210**, 331.

———, 1966, Problems of rock mechanics in petroleum production engineering: Proceedings of the 1st International Society of Rock Mechanics Congress, 585–594.

———, 1973a, A basic theory of subsidence due to reservoir compaction: the homogeneous case: Trans. Royal Dutch Soc. Geol. and Mining Eng, **22**, 43–62.

———, 1973b, Land subsidence above compacting oil and gas reservoirs: JPT, **25**, 734.

Geertsma, J. and G. Van Opstal, 1973, A numerical technique for predicting subsidence above compacting reservoirs, based on the nucleus of strain concept: Verhandelingen Kon. Ned. Geol. Mijnbouwk, **28**, 63–78.

Goodier, J., 1937, On the integration of the thermo-elastic equations: Phil. Mag, **23**, 1017–1032.

Guilbot, J. and B. Smith, 2002, 4-D constrained depth conversion for reservoir compaction estimation: Application to Ekofisk Field: The Leading Edge, **21**, 302.

Hatchell, P. and S. Bourne, 2005a, Rocks under strain: Strain-induced time-lapse time shifts are observed for depleting reservoirs: The Leading Edge, **24**, 1222.

Hatchell, P. J. and S. J. Bourne, 2005b, Measuring reservoir compaction using time-lapse timeshifts: SEG Technical Program Expanded Abstracts, **24**, 2500–2503.

Hatchell, P. J., O. Jorgensen, L. Gommesen, and J. Stammeijer, 2007, Monitoring reservoir compaction from subsidence and time-lapse time shifts in the dan field: SEG Technical Program Expanded Abstracts, **26**, 2867–2871.

Hawkins, K., S. Howe, S. Hollingworth, G. Conroy, L. Ben-Brahim, C. Tindle, N. Taylor, G. Joffroy, and A. Onaisi, 2007, Geomechanical stresses from 4D time shifts measured around the depleting franklin and elgin reservoirs: SEG Technical Program Expanded Abstracts, **26**, 2862–2866.

Hertz, H., 1882, Über die berührung fester elastischer körper.: Journal für die reine und angewandte Mathematik (Crelle's Journal), 156–171.

Hodgson, N., C. MacBeth, L. Duranti, J. Rickett, and K. Nihei, 2007, Inverting for reservoir pressure change using time-lapse time strain: Application to genesis field, gulf of mexico: The Leading Edge, **26**, 649–652.

Holt, R. M., E. Fjær, O.-M. Nes, and J. Stenebrån, 2008, Strain sensitivity of wave velocities in sediments and sedimentary rocks: Presented at the The 42nd US Rock Mechanics Symposium (USRMS), American Rock Mechanics

Association.
Jacoby, W. and P. Smilde, 2009, Gravity Interpretation: Fundamentals and Application of Gravity Inversion and Geological Interpretation: Springer.
Janssen, A. L., B. A. Smith, and G. W. Byerley, 2006, Measuring velocity sensitivity to production-induced strain at the ekofisk field using time-lapse time-shifts and compaction logs: SEG Technical Program Expanded Abstracts, **25**, 3200–3204.
Lakatos, I. and J. Lakatos-Szabo, 2009, Role of conventional and unconventional hydrocarbons in the 21st century: Comparison of resources, reserves, recovery factors and technologies: Presented at the EUROPEC/EAGE Conference and Exhibition.
Landrø, M., 2001, Discrimination between pressure and fluid saturation changes from time lapse seismic data: Geophysics, **66**, 836.
Landrø, M. and J. Stammeijer, 2004, Quantitative estimation of compaction and velocity changes using 4D impedance and traveltime changes: Geophysics, **69**, 949–957.
Lewis, R., K. Morgan, and I. White, 1983, The influence of integration rule accuracy on the calculation of surface subsidence by the nucleus of strain method in conjunction with a finite element reservoir simulator: Applied Mathematical Modelling, **7**, 419–422.
Lumley, D. E., R. A. Behrens, and Z. Wang, 1997, Assessing the technical risk of a 4-d seismic project: The Leading Edge, **16**, 1287–1292.
Lungarini, L., C. Troise, M. Meo, and G. De Natale, 2005, Finite element modelling of topographic effects on elastic ground deformation at Mt. Etna: Journal of Volcanology and Geothermal Research, **144**, 257–271.
Mavko, G., T. Mukerji, J. Dvorkin, et al., 1998, The rock physics handbook, volume **260**: Cambridge University Press Cambridge.
McTigue, D. F., 1987, Elastic stress and deformation near a finite spherical magma body: Resolution of the point source paradox: Journal of Geophysical Research, **92**, 12931–12940.
Mindlin, R., 1949, Compliance of elastic bodies in contact: J. appl. Mech, **16**, 259–268.
Mindlin, R. and D. Cheng, 1950, Thermoelastic stress in the semi-infinite solid: Journal of Applied Physics, **21**, 931.
Minkoff, S., C. Stone, J. Arguello, B. Steve, E. Joe, P. Malgorzata, and W. Mary, 1999, Staggered In Time Coupling of Reservoir Flow Simulation and Geomechanical Deformation: Step 1 – One-Way Coupling: Presented at the SPE 51920 – SPE Reservoir Simulation Symposium.
Mobach, E. and H. Gussinklo, 1994, In-situ reservoir compaction monitoring in the Groningen field: Rock Mechanics in Petroleum Engineering, 29-31 August 1994, Delft, Netherlands.
Mogi, K., 1958, Relations between the eruptions of various volcanoes and the

deformations of the ground surfaces around them: Bull. Earth. Res. Inst., **36**, 99–134.

Nagy, D., 1966, The gravitational attraction of a right rectangular prism: Geophysics, **31**, 362.

———, 2000, The gravitational potential and its derivatives for the prism: Journal of geodesy, **74**, 552.

Nowacki, W., 1986, Thermoelasticity: Pergamon Press Ltd.

Planck, M., 1949, Scientific Autobiography and Other Papers: F. Gaynor.

Rickett, J., L. Duranti, T. Hudson, and N. Hodgson, 2006, Compaction and 4-d time strain at the genesis field: SEG Technical Program Expanded Abstracts, **25**, 3215–3219.

Risnes, R., M. Madland, M. Hole, and N. Kwabiah, 2005, Water weakening of chalk– mechanical effects of water-glycol mixtures: Journal of Petroleum Science and Engineering, **48**, 21–36.

Rogner, H., 1997, An assessment of world hydrocarbon resources: Annual Review of Energy and the Environment, **22**, 217–262.

Røste, T., M. Landrø, and P. Hatchell, 2007, Monitoring overburden layer changes and fault movements from time-lapse seismic data on the Valhall Field: Geophysical Journal International, **170**, 1100–1118.

Røste, T., A. Stovas, and M. Landrø, 2006, Estimation of layer thickness and velocity changes using 4D prestack seismic data: Geophysics, **71**, S219–S234.

Segall, P., 1985, Stress and subsidence resulting from subsurface fluid withdrawal in the epicentral region of the 1983 Coalinga earthquake: Journal of Geophysical Research-Solid Earth, **90**.

Settari, A. and D. Walters, 2001, Advances in coupled geomechanical and reservoir modeling with applications to reservoir compaction: SPE Journal, **6**, 334–342.

Settari, A. T. and V. Sen, 2007, The role of geomechanics in integrated reservoir modeling: The Leading Edge, **26**, 622–627.

Sharma, B. and R. Pilani, 1956, Stresses In an Infinite Slab due to a Nucleus of Thermoelastic Strain in it.: ZAMM-Journal of Applied Mathematics and Mechanics/Zeitschrift für Angewandte Mathematik und Mechanik, **36**, 75–78.

Staples, R., J. Ita, R. Burrell, and R. Nash, 2007, Monitoring pressure depletion and improving geomechanical models of the Shearwater Field using 4D seismic: The Leading Edge, **26**, 636.

Stenvold, T., 2008, Offshore gravimetric and subsidence monitoring: PhD thesis, Norwegian University of Science and Technology, Department of Petroleum Engineering and Applied Geophysics.

Stenvold, T., O. Eiken, and M. Landrø, 2008, Gravimetric monitoring of gas-reservoir water influx – A combined flow- and gravity-modeling approach:

Geophysics, **73**, WA123–WA131.

Tempone, P., E. Fjær, and M. Landrø, 2010a, Improved solution of displacements due to a compacting reservoir over a rigid basement: Applied Mathematical Modelling, **34**, 3352 – 3362.

Tempone, P. and M. Landrø, 2009, Estimation of changes in gravity anomaly due to a compacting reservoir: SEG Technical Program Expanded Abstracts, Houston, **28**, 3790–3794.

Tempone, P., M. Landrø, and E. Fjær, 2010b, 4d gravity response of compacting reservoirs. Submitted to Geophysics.

Tempone, P., M. Landrø, E. Fjær, and N. Inoue, 2009, Effects on time–lapse seismic of a hard rock layer beneath a compacting reservoir: SPE–121081 to be presented at 2009 SPE EUROPEC/EAGE Annual Conference and Exhibition, Amsterdam, The Netherlands, 8–11 June 2009.

Teufel, L., D. Rhett, and H. Farrell, 1991, Effect of reservoir depletion and pore pressure drawdown on in situ stress and deformation in the Ekofisk field, North Sea: Proc. 32" US Symposium on Rock Mechanics, 375–385.

Trasatti, E., C. Giunchi, and M. Bonafede, 2005, Structural and rheological constraints on source depth and overpressure estimates at the Campi Flegrei caldera, Italy: Journal of Volcanology and Geothermal Research, **144**, 105–118.

Tura, A. and D. E. Lumey, 1999, Estimating pressure and saturation changes time-lapse avo data: SEG Technical Program Expanded Abstracts, **18**, 1655–1658.

van Opstal, G., 1974, The Effect of Base-Rock Rigidity on Subsidence Due to Reservoir Compaction: Proc. 3rd Congr. of the Int. Soc. of Rock Mech, 1102–1111.

Walton, K., 1987, The effective elastic moduli of a random packing of spheres: Journal of the Mechanics and Physics of Solids, **35**, 213–226.

Zumberge, M., H. Alnes, O. Eiken, G. Sasagawa, and T. Stenvold, 2008, Precision of seafloor gravity and pressure measurements for reservoir monitoring: Geophysics, **73**, WA133–WA141.

The end